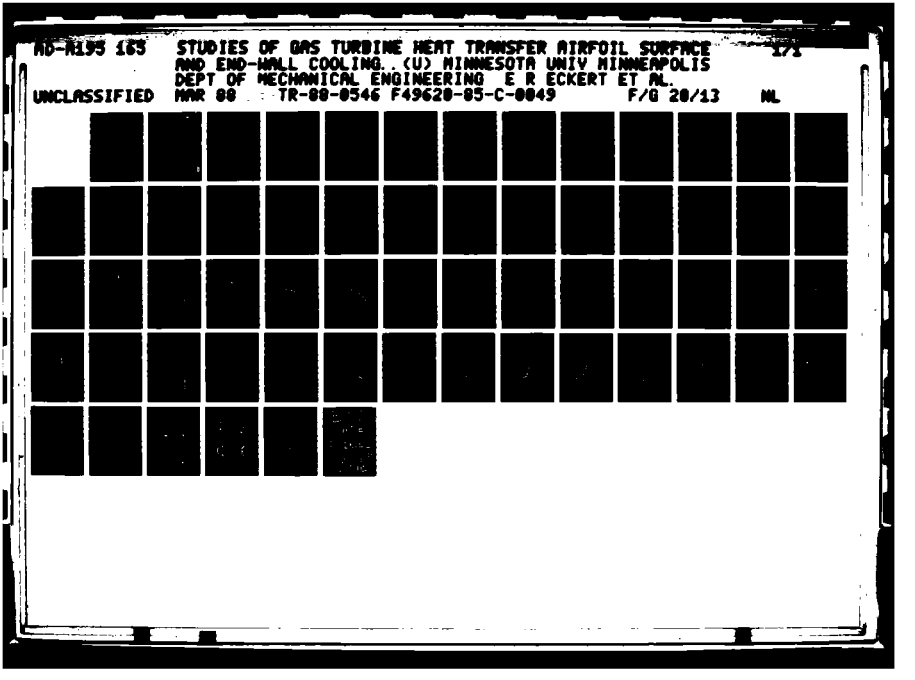
AD-A195 183 STUDIES OF GAS TURBINE HEAT TRANSFER AIRFOIL SURFACE 1/1
AND END-WALL COOLING..(U) MINNESOTA UNIV MINNEAPOLIS
DEPT OF MECHANICAL ENGINEERING E R ECKERT ET AL.
UNCLASSIFIED MAR 88 TR-88-0546 F49620-85-C-0049 F/G 20/13 NL

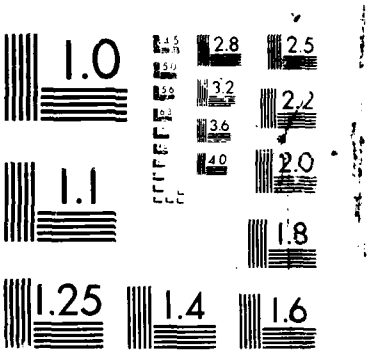

AD-A195 165

REPORT DOCUMENTATION PAGE

DTIC FILE COPY

1b. RESTRICTIVE MARKINGS

2a. SECURITY CLASSIFICATION AUTHORITY

3. DISTRIBUTION / AVAILABILITY OF REPORT

APPROVED FOR PUBLIC RELEASE
DISTRIBUTION IS UNLIMITED

2b. DECLASSIFICATION / DOWNGRADING SCHEDULE

4. PERFORMING ORGANIZATION REPORT NUMBER(S)

5. MONITORING ORGANIZATION REPORT NUMBER(S)

AFOSR-TR- 88-0546

6a. NAME OF PERFORMING ORGANIZATION	6b. OFFICE SYMBOL (If applicable)	7a. NAME OF MONITORING ORGANIZATION
UNIV OF MINNESOTA		AFOSR/NA

6c. ADDRESS (City, State, and ZIP Code)	7b. ADDRESS (City, State, and ZIP Code)
DEPT OF MECHANICAL ENGR MINNEAPOLIS, MINNESOTA 5455	BUILDING 410 BOLLING AFB, DC 20332-6448

8a. NAME OF FUNDING / SPONSORING ORGANIZATION	8b. OFFICE SYMBOL (If applicable)	9. PROCUREMENT INSTRUMENT IDENTIFICATION NUMBER
AFOSR	NA	F49620-85-C-0049

8c. ADDRESS (City, State, and ZIP Code)	10. SOURCE OF FUNDING NUMBERS			
	PROGRAM ELEMENT NO.	PROJECT NO.	TASK NO.	WORK UNIT ACCESSION NO
BUILDING 410 BOLLING AFB, DC 20332-6448	61102F	2307	A4	

11. TITLE (Include Security Classification)
(U) STUDIES OF GAS TURBINE HEAT TRANSFER, AIRFOIL SURFACE AND END-WALL COOLING EFFECTS

12. PERSONAL AUTHOR(S)
ECKERT, GOLDSTEIN, PATANKAR, SIMON

13a. TYPE OF REPORT	13b. TIME COVERED	14. DATE OF REPORT (Year, Month, Day)	15. PAGE COUNT
ANNUAL	FROM 03/87 TO 03/88	03/88	58

16. SUPPLEMENTARY NOTATION

17. COSATI CODES			18. SUBJECT TERMS (Continue on reverse if necessary and identify by block number)
FIELD	GROUP	SUB-GROUP	
			HEAT TRANSFER, TURBULENCE

19. ABSTRACT (Continue on reverse if necessary and identify by block number)

Research results on curved surface heat transfer, airfoil heat transfer, film cooling and end-wall heat transfer are presented. In particular these studies focus on the recovery process of a turbulent boundary layer from curvature, heat transfer measurements and numerical prediction techniques of film-cooling on an adiabatic flat plate by injection through a single row of holes.

DTIC ELECTE MAY 19 1988 D

20. DISTRIBUTION / AVAILABILITY OF ABSTRACT	21. ABSTRACT SECURITY CLASSIFICATION
☐ UNCLASSIFIED/UNLIMITED ☒ SAME AS RPT ☐	UNCLASSIFIED

22a. NAME OF RESPONSIBLE INDIVIDUAL	22b. TELEPHONE (Include Area Code)	22c. OFFICE SYMBOL
HENRY E HELIN, CAPTAIN, USAF	202-767-0471	AFOSR/NA

DD FORM 1473, 84 MAR 83 APR edition may be used until exhausted.
All other editions are obsolete.

SECURITY CLASSIFICATION OF THIS PAGE
UNCLASSIFIED

AFOSR-TR- 88-0546

Annual Progress Report
1 March1987 - 30 April 1988

Studies of Gas Turbine Heat Transfer
Airfoil Surface and End-Wall Cooling Effects

AFOSR Grant # F49620-85-C-0049

Co-Principal Investigators:

E. R.G. Eckert — Date

R. J. Goldstein — Date

S. V. Patankar — Date

T. W. Simon — 4/14/88 Date

March 1988

INTRODUCTION

Following our Annual Progress and Forecast Report of January 1988, this report is prepared to present research activities at the Heat Transfer Laboratory of the University of Minnesota under AFOSR sponsorship, for the period of 1 March1987 - 30April 1988. The research topic is heat transfer from gas turbine airfoil and endwall. The report is divided into subtopics: A- Recovery of a turbulent boundary layer form curvature, B- Turbine blade heat transfer, C- Film cooling, D- Numerical prediction of film coooling on an adiabatic flat plate by injection through a single row of holes, E- Heat transfer near the base of a protruding cylinder, and F- The two -half-blade cascade test.

A. RECOVERY OF A TURBULENT BOUNDARY LAYER FROM CURVATURE

INTRODUCTION

The following describes an experiment to determine the processes by which a turbulent boundary layer relaxes from concave curvature in the presence of elevated free-stream turbulence intensity and streamwise pressure gradient for two radii of curvature. This boundary layer, grown on a uniform radius of curvature developing section, has been allowed to undergo transition naturally. Two radii of curvature will be investigated, 180 cm and 90 cm. The effect of three levels of free-stream turbulence will be investigated (approximately 0.5%, 2%, and 10%). Runs with a streamwise pressure gradient will be made under constant-β conditions and with an acceleration profile which is representative of the gas turbine blade pressure-side boundary layer pressure gradient profile. This investigation will be done in a unique heat transfer test facility which has walls that can be bent to various radii of curvature.

Measurements are to be made of the local convective heat transfer coefficient and profiles of mean velocity and temperature, streamwise turbulence intensity, Reynolds shear stress ($\overline{u'v'}$), the turbulent diffusion of heat ($\overline{v't'}$), and intermittency. A liquid crystal sheet, presently in place, is used to visualize steady or slowly varying spanwise nonuniformities (streaks) and streamwise roll cell vorticies (Taylor-Goertler vorticies) expected in the

boundary layer on the concave developing wall, and may be useful in visualizing any vorticies on the recovery wall. The liquid crystal visualization has already proven, in this facility, to be useful for visualizing any unwanted secondary flow effects that may be present.

Particular emphasis will be placed on documenting scales in the flow. Measurements to be taken within the boundary layer include the autocorrelation, all three components of the turbulence intensity, and two-point correlations with cross-stream probe separation.

OBJECTIVES

The study is to begin with a baseline case on a curved wall of 180 cm radius of curvature with no streamline acceleration and a low free-stream turbulence intensity (0.5%). All subsequent runs will be compared to this case so that the effects of pressure gradient, turbulence intensity, and curvature on recovery can, at first, be isolated. The proposed test matrix is shown on Table A-1. The acceleration runs will be made with constant ß values (self-similar). Cases will be added where the acceleration values simulate those of the turbine blade pressure side with elevated turbulence intensity levels (10%), simulating blade conditions. Additional cases of combined effects may be also be included, as appropriate.

1	0.45	-180	No	45° bend, low TI, no acc.
2	2.0	-180	No	45° bend, mid TI, no acc.
3	0.45	-90	No	90° bend, low TI, no acc.
4	2.0	-90	No	90° bend, mid TI, no acc.
5	2.0	-90	Yes	90° bend, mid TI, acc.
6	10.	-90	Yes	90° bend, high TI, acc.

Table A-1 - Test Matrix

The free-stream turbulence characteristics will be well documented. Measurements of $\overline{u'}$, $\overline{v'}$, and $\overline{w'}$ in the free-stream will be made where appropriate using a triple-wire. Measurements of the auto-correlation and scales in the flow will be made. The measurements program consists of measuring, as a minimum, the following quantities:

1). Mean and fluctuating components of streamwise velocity. Mean velocities are measured using a pitot tube in the

heated flow, and mean and fluctuating velocities are measured by a horizontal hot-wire in isothermal flows.

2). Mean temperature profiles. The thermocouple probe described by Wang and Simon (1987) will be used.

3). Local Stanton number. Embedded thermocouples in the test wall are for this purpose.

4). Shear stress profiles and profiles of the fluctuating component of cross-stream velocity will be documented in isothermal flows where the flow is sufficiently two-dimensional. A cross-wire probe will be used for these measurements.

5). Transverse velocity correlation coefficients in the free-stream as well as profiles of the autocorrelation of streamwise velocity will be measured. Two horizontal hot-wire probes will be used for the transverse measurements and a horizontal wire will be used for the autocorrelation.

6). Intermittency. A horizontal hot-wire placed in the wake region of the boundary layer is used to determine when the flow is rotational or irrotational. An analog intermittency function will be generated so that processing based upon the state of the flow (rotational or irrotational) can proceed as appropriate. An analog intermittency function is merely an analog signal that is 0 if the flow is irrotational and 1 if the flow is rotational.

7). Measurements of the turbulent heat flux $\overline{v't'}$ in the boundary layer will be made where the flow is two-dimensional. A triple-wire probe has been developed for this purpose.

If the boundary layers are sufficiently thick and the flow is three-dimensional, measurements of the three components of velocity along with their cross-correlations will be made with a triple wire.

WORK COMPLETED TO DATE

The tunnel has been modified since the completion of the convex wall study by putting in a computer-actuated fan controller and a settling chamber upstream of the screen pack. A bendable test wall designed for the concave curvature developing section has been designed, constructed and installed. The tunnel and this test wall have been qualified. The recovery wall is of similar design, and has been used in a previous study (You, Simon, and Kim--1986a,b). A schematic of the test facility is shown on Fig. A-1.

Mean velocity and streamwise turbulence intensity measurements within the potential core of the flow exiting the nozzle showed a peak-to-peak variation in velocity of 0.2% about a nominal velocity of 27 m/s and turbulence intensity of 0.5%. Measurements of mean temperature within the flow exiting the nozzle showed a peak-to-peak variation of 0.02°C.

Qualification of the developing section in the flat wall configuration with regard to transition location was performed by heating the wall and visualizing transition using the liquid crystal sheet. Transition occurs at the location where the liquid crystal first changes color as the heat flux is gradually increased. This corresponds to the highest wall temperature, or, since the wall heat flux is essentially uniform, the location of lowest heat transfer coefficient. Various parameters such as the leading edge suction flow rate and the suction slot width were optimized such that transition occurred as far downstream as possible for a given free-stream velocity and turbulence intensity. The outer flexible wall was adjusted such that there was no pressure gradient along the wall.

The Reynolds numbers based on displacement and momentum thickness at the beginning of transition were measured to be 1920 and 737, respectively. The free-stream turbulence intensity was measured to be 0.43%. A plot of the Reynolds number based on displacement thickness vs. the free-stream turbulence intensity for the present study is shown on Fig. A-2, and is seen to be in excellent agreement with the data of other researchers.

An energy balance was performed by integrating the wall heat flux along the centerline of the test wall and comparing this with the increase in energy carried in the boundary layer flow as calculated from the mean velocity and temperature profiles. The closure was to within 3%.

Further qualification of the developing test section and measurement techniques were performed by comparing data

measured in the flat wall transitional flow with that of other researchers. Measurements of Stanton number, St, mean velocity and temperature profiles, shape factor, H, and the intermittency (fraction of total time the boundary layer flow is turbulent-like), γ, are shown on Figs. A-3 through A-7, respectively. This data all seems to be in agreement with other researchers' results.

Determination of the skin friction coefficients in the transition region poses some problems in that no technique comparable to the Clauser technique is available. Virtually the only way of measuring skin friction coefficients in transitional boundary layers is to directly determine the shear stress at the wall by measuring the near wall velocity gradient. This necessitates measuring the velocity profile very near the wall. The wire of a hot-wire probe (TSI 1218-T1.5 horizontal boundary layer probe) was remounted on the tips of the probe prongs such that as the probe is traversed toward the wall, the wire touches the wall first. A cathetometer was used to view the approach of the wire to the wall, and to make sure that both prongs touch the wall simultaneously. After placing the wire as close to the wall as possible, the wire was backed away in 10 micrometer increments (one division on the micrometer) while the near-wall data was taken. This technique enabled the near-wall velocity gradient, and thus the near-wall shear stress, to be determined. Streamwise variation of the skin friction coefficient on the wall is shown on Fig. A-3 (the Stanton number variation measured using embedded thermocouples in the wall is also shown in this figure). This probe will be useful in the study of the boundary layer recovering from concave curvature in that it will allow a more detailed investigation of the sublayer region of the boundary layer. In particular, we wish to study the curvature and elevated free-stream disturbance level effects on the near-wall region.

The circuit for producing an intermittency function has been constructed (see Fig A-8). It exploits the large difference between the time-derivative of a turbulent-like flow and that of a laminar-like flow. In this circuit, the derivative of the hot-wire anemometer signal is compared to a threshold value. If the time-derivative is greater than the threshold, the flow is declared turbulent. The second derivative of the signal with respect to time is also used. The threshold of this signal is chosen so that "zero crossing" error is avoided. The "zero crossing" error occurs when the time-derivative of a turbulent signal passes through the band where the absolute value of the signal is below the threshold value (see Fig A-9). The circuit, without the second derivative, would declare the flow laminar during this time even though it is clearly turbulent. To

avoid this problem, both the first and second derivative are examined and the flow is declared turbulent if either signal is higher than the threshold value (bottom trace of Fig. A-9). This circuit has been constructed and is waiting to be tested and to be tuned to accommodate the voltage ranges occurring in the test. The intermittency produced by the circuit will be compared to an intermittency computed by the current method which samples the signal and holds its digitized values in the buffer of a storage oscilloscope. Once the buffer is full (about four-thousand samples) these values are transferred to a computer where the derivative is numerically calculated and compared to a threshold. Values above the threshold represent turbulent flow values. The ratio of the time that the flow is turbulent-like to the total time sampled is the intermittency of the flow. Although this method is reliable, it is too time-consuming due to the long transfer times required to move the data from the oscilloscope to the computer. The circuit described above is expected to make the determination of the intermittency function a routine measurement. It also allows a continuous signal indicating regime, laminar or turbulent, rotational or irrotational, without digitizing the great amount of data required to capture the signal waveform. The intermittency measuring unit will be used to separate the turbulent and laminar or rotational and irrotational, contributions to various parameters e.g. velocity, turbulent normal and shear stresses, thermal transport of heat, $\underline{v't'}$, etc. This will be an easy task since the intermittency function will be recorded along with the u', v' and t' data. The determination of the turbulent and laminar or rotational and irrotational contributions will be valuable to turbulence model researchers

A probe to measure $\underline{v't'}$ in turbulent boundary layers was developed by Kim and Simon (1988) and used to take measurements in a turbulent boundary layer over a convex surface with recovery. In the method used for this probe, two parallel wires operating at different overheat ratios were used to deduce the instantaneous temperature in the flow. Due to inconveniences with the operation of this probe, however, it was decided to change the scheme to one where we operate one of the wires in the constant-current mode as a resistance thermometer to measure the instantaneous flow temperature, and the other as a standard constant-temperature wire. The method of Hishida and Nagano (1978) was chosen for compensation for the low frequency response of the constant-current cold-wire. In this method, the heat transfer coefficient over the constant-current cold wire is estimated from the parallel hot-wire

signal. The cold-wire signal as well as its time derivative is used in the signal processing using this method. A circuit built for this purpose is shown on Fig. A-10 A current source which can be switched from 1 mA to 30 mA drives the cold-wire. The 30 mA current level is needed to heat the wire substantially. This is necessary for determining the thermal frequency response of the wire as the wire cools to essentially room temperature as the current is switched from 30 mA to 1 mA. The resistance is sensed using the 1 mA current level. The voltage across the wire is amplified 1000 times, then sent through a differentiator. The noise requirements on the circuit are very tight. Although the cold-wire has a nominal resistance of 5 Ω, the variation of wire-resistance within the heated boundary layer is only expected to be 0.005 Ω rms at most. For a nominal wire-current of 1 mA, this corresponds to only a 5 μV rms variation. The circuit noise must be much smaller than this to get an adequate signal-to-noise ratio. The noise of the amplifier is presently 0.5 μV rms referred to input, implying a signal-to-noise ratio of 10; the signal-to-noise ratio at the exit of the differentiator is 3. Careful attention to minimizing the potential for ground loops is essential to obtaining these values. A profile of the temperature fluctuation in a turbulent boundary layer taken with the probe/circuit is shown on Fig. A-11. The data is seen to be in good agreement with that of Gibson and Verriopoulos (1984) and Blair and Bennett (1984). Measurements of $\overline{v't'}$ in a transitional boundary layer are presently being taken.

A study has been initiated to look into various methods of generating and characterizing higher levels (10%) of free-stream turbulence. The effects of various grid geometries and grid configurations on the free-stream turbulence are under investigation. Three-wire hot-wire measurements to characterize the turbulence structure are being incorporated. The most successful technique will be used to generate a higher level of free-stream turbulence for the investigations of the free-stream turbulence effects on transition and the recovery from curvature processes.

The recovery wall in the concave curvature-study will be the same one used in the convex-wall study recently completed. The concave (flexible) wall, now in a straight configuration, is presently in use for a boundary layer transition study. Drawings, showing how the recovery wall will be connected to this concave wall are now being made (see Fig A-12). A separate, intermediate, composite wall will be constructed to provide a smooth transition from the curved wall to the main recovery wall. The heater will extend far enough on

both sides, so that there will be continuous heating from the concave wall to the recovery wall. This is done to avoid any unheated length which would influence the recovery of the thermal boundary layer. A liquid crystal sheet will be layed on the heater covering all three walls; curved, intermediate, and recovery. This will give a hydrodynamically smooth surface for the recovery of the boundary layer. As presently planned, the recovery wall will be connected to the flexible concave wall while it is still in the straight configuration. If done this way, a base case for determining the suitability of the recovery wall will be provided.

Now that the developing section test wall has been qualified, the program will proceed to qualifying the recovery section test wall. No major problems are anticipated during this qualification since the test wall has already been qualified in a previous study. All measurements, discussed above, that are required for this baseline case can be taken.

B. TURBINE BLADE HEAT TRANSFER

To design and manufacture more efficient, durable, and economical gas turbines precise information is needed on the performance of component of a turbines. One of the most sensitive parts of a gas turbineis the first stage blade. Turbine blades are often damaged due high temperature and load. Sometimes the damage is local because of high local heat transfer.To diminish the possibility of blade failure designers need to know the distribution of heat transfer coefficient over a blade. This knowledge could be acquired through numerical modeling of the flow and heat transfer, if the model were capable of giving reasonably accurate results. Preparation of a numerical model and the accuracy of its outcome are heavily dependent on comparison with test data over a range of conditions. To meet this end a series of basic experimental studies were undertaken.

A mass transfer technique is used to determine the heat transfer distribution over pressure and suction side surfaces of a turbine blade in a linear cascade. A newly developed computer aided data acquisition system is employed to obtain many data points in a relatively short period. This provide a dense array of precise local measurements which were not possible before.

Measurements are carried out both in two and three dimensional regions of the flow around the blade. Two dimensional measurements are performed to check the data acquisition system

and the test set up against already available data.Three dimensional measurements are taken to furnish the needed data for the most prevailing operating conditions of the modern turbines. Typical two dimensional measurements on the convex surface are shown in Figs. B-1 & B-2. These figures show the spanwise distribution of the Sherwood number (equivalent to Nusselt No. in heat transfer) at selected streamwise locations over the blade surface. The span of the blade covered in these measurements is far from the end-wall ($Z/C > 5$ where Z is the distance along the blade span measured from the end-wall and C is the cord length). Comparison of these figures indicates that mass (heat) transfer coefficients are practically spanwise constant accross the span for streamwise locations less than about 80 % of the cord ($S/C < 0.80$, S is the curvilinear distance along the blade surface measured from the stagnation point). At locations $1.13 < S/C < 1.27$, a substantial variation with Z in the Sherwood number is observed. This is believed to be due to three dimensional effects of laminar separated flow near the trailing ede average Sherwood number, shown on Fig. B-3 at about $S/C = 1.1$, is also an indication of this laminar separated region. The rapid increase of mass transfer for $1.1 < S/C < 1.18$ indicate that flow progresses through transition and reattachment. Present measurements are also compared (Fig. B-3) with a set of data *reported in the* literature and the agreements, considering the differences in experimental conditions, are good Fig. B-3.

Mass transfer measurements are also carried out in the three dimensional region of the flow, where the influence of the end-wall is strong. A representative distribution of these data is shown on Fig. B-4. These datashow that near the leading edge mass (heat) transfer is two dimensional over most of the blade span. Three dimensional effects, however, do appear farther downstream. These effects are due to the secondary flows through the passage between adjacent blades. In the region $0.9 < S/C < 1.335$, the effect of the secondary flows are present for a distance along the blades span. Distributions of the local mass transfer along the span at several streamwise locations are shown on Figs. B-5 and B-6 . Figure B-6 is the near end-wall enlargement of figure B-5. The peak of heat transfer close to the end-wall is indicative of the existence of a corner vortex at the junction of the blade and the end-wall. As it is expected, the location of the peak moves away from the wall in flow direction pointing to the lift up of the vortex. Existence and lift up of this corner vortex were also observed in a previously reported study of heat transfer from the end-wall.

Presently, the information gathered through this study is being analyzed and put together for publication; meanwhile, the test set up is being modified and corrected for mass transfer measurements to be taken on a blade's concave surface

C - FILM COOLING

Film cooling is extensively used to protect gas turbine blades against the very high temperature gases flowing over them. Numerical modeling of the film cooling, though successful in limited flow conditions, still requires further refinements. The refinements, and the applicability of numerical model to the actual flow environment, can only be achieved through detailed knowledge of the prevailing flow and heat transfer process. One of the factors making the actual process different from the settings of most of the available data is the effect of the turbine blade surface curvature. To handle this problem in a reasonable fashon, a series of experimental investigations are devised to detect the influencing prameters and their behavior. One such study considered film cooling through a row of holes on a concave and a convex surface. Local measurements of effectiveness under varying wall curvature and injection parameters are examined. Results of this study have already been reported and are being prepared for journal publication. In this study injection angle was fixed at 35 degrees relative to the mainstream. One outcome of this investigation was to notice that on the concave surface, partly due to the dominance of tangential momentum flux, the effectiveness is almost two dimensional. This observation led to the decision of quantifying the effect of varying injection angle on the performence of film cooling over curved surfaces. To this end, the flow structure on the curved surface must be defined.

Measurements of the flow field at first indicated a highly three-dimensional structure; however, a defective tripwire and a poorly placed impact probe were found to be the problem. The time-mean two-dimensional nature of the flow field has now been confirmed. Figure C-1 shows the undisturbed velocity profiles at the points of injection; Table C-1 gives the measured integral parameters.

Work has also been done to develop a boundary-layer mixing model to correlate spanwise-averaged effectiveness data for concave walls. This is thought to be workable by virtue of the intense mixing levels characteristic of a turbulent, concave-wall boundary layer. Two deviations from similar flat-plate models include the inaccuracy of a 1/7th power profile assumption, and the increased rate of

growth undergone by boundary layers on concave walls (i.e. d > 0.37/Re**0.2) This topic will be further explored during the planned flow visualization trials, when direct information about jet penetration will be available.

Finally, the experimental apparatus itself is now fully built. This includes the machining of an additional injection plate where a uniform of spanwise injection will be measured (all other tests will involve injection at various angles in line with the freestream). Qualification tests are getting underway at the time of this writing.

Table C-1. NOMINAL OPERATING CONDITIONS

	CONVEX		CONCAVE	
	current measurements	previously reported	current measurements	previously reporte
T	21 C	24 C	21 C	24
Ubar	41 m/sec	40 m/sec	41 m/sec	40 m/sec
d99	3.30 cm	0.89 cm	2.29 cm	2.28 c
d1	0.25 cm	0.11 cm	0.46 cm	0.41 cm
d2	0.14 cm	0.09 cm	0.34 cm	0.29 cm
H	1.74	1.22	1.37	1.41

NOTE: The calculation procedure used for the current measurements differs from that used previously. In the current method, the variation of static pressure across the boundary layer is taken into account through direct measurements, whereas in the previous computations the static pressure was assumed to be constant across the boundary layer. This is thought to account fully for the discrepancy in the previous data near the concave wall.

The rather striking disagreement on the convex wall can be readily understood through Fig. C-1. One point to note is that previously the edge of the boundary layer was defined at about R = 4.35 inches, whereas now it is defined at R = 5.30 inches.

D. NUMERICAL PREDICTION OF FILM COOLING ON AN ADIABATIC FLAT PLATE BY INJECTION THROUGH A SINGLE ROW OF HOLES

INTRODUCTION AND OBJECTIVES

High temperature of gases lead to significant increase in output and economy in gas turbine systems, but these high temperatures have detrimental effect on the surfaces exposed to the gases. Most widely used method to locally cool the exposed surface is injection of low temperature coolant through rows of holes. Since, slot cooling (two dimensional) is not practicable in most applications, injection film cooling through row(s) of holes is more practical and popular. The effectiveness of the three dimensional film cooling is significantly lower than the slot injection cooling because the hot mainstream fluid can flow underneath the injected jet due to the secondary flow in the cross stream direction. In spite of a large amount of experimental effort to study this complicated flow and heat transfer situation, it is still not a well understood phenomenon. Many studies site the effects of mainstream turbulence intensities, turbulence scales, blowing rates, injection hole geometries, mainflow and injection Reynolds numbers on the film cooling effectiveness on an adiabatic wall. Some experimental works have also been reported on the effects of the nature of injection viz. injection angle, injection Reynolds number, turbulence intensities and scales, and injection velocity profiles on the cooling effectiveness.

An attempt to study the injection film cooling through a row of holes. using the three dimensional parabolic numerical scheme (Patankar and Spalding, 1972) is made. The details, advantages and the limitations of this approach is discussed in subsequent sections. Comparison with experimental results and effects variation in the main stream turbulence intensities, turbulence scales and injection mass flow rates on the adiabatic wall temperature are being presented. The report also demonstrates the successful extension of the regular K-e model to this complex problem. Further, this approach can be extended to study the injection jet characteristics and their interaction with the mainstream flow in detail, complex injection geometries, and curvature of the adiabatic walls. Presently, work on injection through two rows of holes in a staggered configuration is underway.

PROBLEM DESCRIPTION

The problem considered is a mainstream flow with uniform inlet velocity of 30 m/s over an adiabatic flat plate with injection at an angle of 35 degrees to the plate through a single row of holes 1.092 cms in diameter. The Reynolds number based on injection tube diameter has been kept constant at 21000 throughout this study. The

injection holes are separated in the transverse direction by three diameters of the injection tubes. Blowing rate, M (defined in this report the ratio of injection velocity to the main stream velocity, neglecting the compressibility effects) is a parameter and tests for the values of 0.5, 1.0, and 1.5 were conducted. It is evident that all the above mentioned parameters can be varied simultaneously, one at a time or in any combination the investigator deems necessary and appropriate results can be obtained with extreme ease. Care has been taken to ensure that the flow is fully developed before the injection, to maintain consistency with the experimental practice. The temperatures of the mainflow and the injectant flow are 100 and 65 degrees centigrade respectively. The injecting jet in this preliminary study is a turbulent flow with a uniform velocity profile across the cross-section of the injecting tube. For further studies on the details of the injection jet and mainstream interaction, a more realistic fully developed profile can be incorporated. In the numerical scheme the profile is an input quantity, so theoretically, any injection profile can be prescribed and studied.

The row of equally spaced holes facilitates the choice of a computational domain covering the plane of the centerline of one hole to the midplane between that hole and an adjacent hole. The entire problem domain is symmetric about both these planes. This prescription save both computer storage and effort. The upper boundary is assumed to be far from the wall so that no influence of the upper boundary is felt by the flow near the wall. A non-uniform grid is adopted in the domain discretization, so that more grid points are packed near the wall and the hole.

GOVERNING EQUATIONS AND TURBULENCE MODEL

The governing equations for time-independent, three-dimensional turbulent flow in terms of the time-averaged quantities in the cartesian tensor notation are as follows:

Continuity equation:

$$\frac{\partial}{\partial x_i}\left(\rho \overline{u}_i\right)=0 \qquad (1)$$

Conservation of momentum:

$$\frac{\partial}{\partial x_j}\left(\rho \overline{u}_i \overline{u}_j\right) = \frac{\partial}{\partial x_j}\left(\mu \frac{\partial}{\partial x_j} \overline{u}_i - \rho \overline{u'_i u'_j}\right) + S_i - \frac{\partial p}{\partial x_j} \qquad (2)$$

Conservation of thermal energy:

$$\frac{\partial}{\partial x_j}\left(\rho \overline{u}_i \overline{T}\right) = \frac{\partial}{\partial x_j}\left(\Gamma \frac{\partial \overline{T}}{\partial x_j} - \rho \overline{u'_i T'}\right) + S_h$$

(3)

The Reynolds stress term in equation (2) is expressed in terms of turbulent viscosity μ_t as:

$$-\rho \overline{u'_i u'_j} = \mu_t \left(\frac{\partial}{\partial x_j} \overline{u}_i + \frac{\partial}{\partial x_i} \overline{u}_j\right) - \frac{2}{3}\delta_{ij}\left(\mu_t \frac{\partial}{\partial x_l} \overline{u}_i + k\right) \qquad (4)$$

An effective pressure is defined by including the second term in the equation (5) with the pressure in the momentum equation (2):

$$P = p - \frac{2}{3}\left(\mu_t \frac{\partial}{\partial x_l} \overline{u}_i + k\right)$$

The real viscosity of the fluid is assumed uniform and thus the source term S=0. The momentum equation thus can be written as:

$$\frac{\partial}{\partial x_j}\left(\rho \overline{u}_i \overline{u}_j\right) = \frac{\partial}{\partial x_j}\left(\mu \frac{\partial}{\partial x_j} \overline{u}_i\right) - \frac{\partial P}{\partial x_j} + \frac{\partial}{\partial x_l}\left(\mu_t\left(\frac{\partial}{\partial x_j} \overline{u}_i + \frac{\partial}{\partial x_i} \overline{u}_j\right)\right) \qquad (5)$$

The convention adopted in this section is a cartesian coordinate system with X as the mainstream direction, Y and Z in the cross-stream directions and u, v, and w are the corresponding time averaged velocities. Under the parabolic assumption, the gradients of all quantities (except pressure) in the mainstream direction are considered small compared to the gradients in the cross-stream directions. The general momentum equation can be further simplified to

$$\frac{\partial}{\partial x_j}\left(\rho u_i u_j\right) = \frac{\partial}{\partial x_j}\left(\mu_{eff}\frac{\partial}{\partial x_j}u_i\right) - \frac{\partial P}{\partial x_i} + S_i \qquad (6)$$

where,

y-momentum $\quad S_i = \left(\frac{\partial \mu_t}{\partial z}\right)\frac{\partial w}{\partial y} - \left(\frac{\partial \mu_t}{\partial y}\right)\frac{\partial w}{\partial z}$

z-momentum $\quad S_i S_i = \left(\frac{\partial \mu_t}{\partial y}\right)\frac{\partial v}{\partial z} - \left(\frac{\partial \mu_t}{\partial z}\right)\frac{\partial v}{\partial y}$

x-momentum $\quad S_i = 0$

and effective viscosity $\quad \mu_{eff} = \mu_t + \mu$

in the energy equation(3) we define the turbulent term

$$-\rho\,\overline{u'_i T'} = \Gamma_t \frac{\partial T}{\partial x_i}$$

where

$$\Gamma_t = \frac{\mu_t}{pr_t}$$

and since $\mu_t >>> \mu$

$$\Gamma_{eff} = \frac{\mu_t}{pr_t}$$

The energy equation without the source term is then

$$\frac{\partial}{\partial x_i}\left(\rho\,\overline{u}_i\,\overline{T}\right) = \frac{\partial}{\partial x_i}\left(\Gamma_{eff}\frac{\partial \overline{T}}{\partial x_i}\right) \qquad (7)$$

<u>The boundary conditions :</u>

$$\frac{\partial u}{\partial y} = 0, \quad v = 0, \quad \frac{\partial w}{\partial y} = 0, \quad \frac{\partial T}{\partial y} = 0 \quad \text{at } y = 0 \text{ and } y = yl$$

(symmetric -

boundary)

$v=0$, $w=0$, $u=0$ at z=0 (wall boundary)

$\frac{\partial u}{\partial z} = 0$, $\frac{\partial v}{\partial z} = 0$, $w=0$ at z=zl (symmetric boundary)

in the injection zone (at z=0)

$u = u_{inj} \cos(\beta)$
$w = w_{inj} \sin(\beta)$

The initial conditions:

u=uin, v=0, w=0, and T=Tin at all y and z at x=0

The k-ε turbulence model:

This differential model is used to estimate the turbulent viscosity or equivalently the turbulent Reynolds stress in momentum equation formulation.We need to solve additional transport equations for the turbulent kinetic energy k and dissipation ε .The equations describing the model are presented here for the steady case.

$$\mu_t = \frac{C_\mu \rho k^2}{\varepsilon} \qquad (8)$$

$$\frac{\partial}{\partial x_i}\left(\rho u_i k\right) = \frac{\partial}{\partial x_i}\left(\frac{\mu_t \partial k}{\sigma_k \partial x_i}\right) + G - \rho\varepsilon \qquad (9)$$

$$\frac{\partial}{\partial x_i}\left(\rho u_i \varepsilon\right) = \frac{\partial}{\partial x_i}\left(\frac{\mu_t \partial \varepsilon}{\sigma_\varepsilon \partial x_i}\right) + (G\,C_1 - \rho\varepsilon C_2)\frac{\varepsilon}{k} \qquad (10)$$

where,

$$G = \mu_t\left(\frac{\partial}{\partial x_j}u_i + \frac{\partial}{\partial x_i}u_j\right)\frac{\partial}{\partial x_j}u_i$$

and the empirical constants of the regular k-e model are :

C_1=1.44, C_2=1.92, C_μ=0.09
σ_k=1.0, σ_ε=1.3

The boundary conditions are as follows:

$\frac{\partial k}{\partial z} = 0, \quad \frac{\partial \varepsilon}{\partial z} = 0$ z=zl (symmetric boundary)

$\frac{\partial k}{\partial z} = 0$ z=0 (wall boundary)

$\frac{\partial k}{\partial y} = 0 \quad \frac{\partial \varepsilon}{\partial y} = 0$ at y=0 and y=yl (symmetric boundary)

while in the injection zone on the wall (z=0)

k=kinj and ε=εinj

the initial conditions at x=0 are k=kin and ε=εin

The turbulent viscosity is much greater than the real viscosity for most part of the flow, but near the wall both the viscosities are comparable. Here we use the wall functions to deduce the effective viscosity in the near wall region. The k-ε turbulence model has been successfully tested for many problems in two dimensions and a few three dimensional cases. The effectiveness of the model in capturing this three dimensional mixing phenomenon is being tested in this work.

The three dimensional parabolic solution procedure developed by Patankar and Spalding (1972) is used to solve the five transport equations introduced in this section. The cross-stream pressure distribution in and around the injection zone will be non-uniform leading to large amounts of secondary cross-stream flow. But this method computes an average effective pressure gradient uniform over the cross-section while in reality the flow near the jet will have non-inform pressure gradients. The errors introduced by this step

will be serious if the parabolic assumption for the flow breaks down. As the results will show, the effects of the errors in the pressure gradient computations are limited to the zone very close to the injection port. It is this pressure computation that allows the development of the marching procedure which saves large amounts of computer effort and memory compared to a full-scale three-dimensional solution procedure.

RESULTS AND DISCUSSION

The aim of the film cooling investigators is to control, predict and study the adiabatic wall temperature under various flow situations. This adiabatic wall temperature is expressed by a dimensionless temperature called the film cooling effectiveness, defined as:

$$h = (T_{aw} - T_{inf}) / (T_c - T_{inf})$$

where Taw is the adiabatic wall temperature, Tinf is temperature of the hot main stream and Tc is the cooler injectant temperature. The results presented in this section show the effects of the variation in some parameter on the film cooling effectiveness.

a) The primary test of validating the computational results is through comparison with the available existing body of experimental data in the field. Figure D-1 shows the numerically predicted film cooling effectiveness downstream of the injection port compares well with the experimental data of Goldstein, Eckert, Ericksen, and Ramsey. The comparison has been done for the other cases as well (when the data were available) This result demonstrates that this numerical approach is capable of successfully capturing the phenomenon except in the regions very close to the hole. This is expected since we use a parabolized marching process, while the actual flow in this region is not parabolic. There would be local recirculations and flow reversals just downstream of the hole, but for angular jets where the injection angles are less than 35 degrees, these effects are considerably small and localized very near (less than 2 or 3 hole diameters). This region of complex flow is difficult to access even in an experimental setup, and its effects down stream are minimal, hence the choice of the solution procedure. A detailed study of near injection needs many times more computational effort and memory and so would not be advantageous for this class of problem.

b) The effects of variation in the free-stream turbulent kinetic energy on the centerline cooling efficiency at various locations downstream is shown in the figure D-2.The result is then compared to the experimental data of Kadotani and Goldstein in D-3, showing a good agreement The three cases studied were mainstream **k** equaling 1%, 5%, and 10% of the mainflow velocity, and from figure D-2 cooling effectiveness shows a large degree of insensitivity. For medium blowing rates of M=0.5, which was adopted in this study, the degree of penetration of the injectant into the main flow is of the same order as the turbulent boundary layer thickness. This accounts for the attained insensitivity. For a more detailed analysis of the effects free-stream turbulence intensities cases with different blowing rates and different Reynolds numbers must be studied and is a part of the near-term plan.

c) The sensitivity of the centerline cooling effectiveness to the changes in free-stream dissipation (which is proportional to the Reynolds number based on the turbulent viscosity and is a quantity which scales on the turbulence scale of the flow) is shown in the figure D-4 As in the previous sensitivity study, the cooling effectiveness is insensitive to variations in free-stream ε , and for the same reasons. It is evident from these two studies that a more indepth analysis for different blowing rates must be done to confirm and extend the ideas gathered so far from the experimental works.

d) The figure D-5, extends the observation in (c) for a higher injection mass flow rate (M) of 1.0. The sensitivity of the effectiveness to the variations in the mainstream turbulence scale is not appreciable. The magnified view of this test for a region between 5 and 35 diameters downstream is shown in the figure D-6. An increase in the effectiveness with the variation in the turbulence scale (Reynolds number based on this scale 250, 500 and 1000 in the three cases) is noticed but not significant. This insensitivity of the effectives to variations in the main stream turbulence scale cannot be conclusively claimed without further investigation.

e) The effect of increase in in the injection mass flow rate on the film cooling effectiveness is shown in the figure D-7. The increase in the injection velocity decrease the effectiveness downstream of injection. This is attributed to the higher degree of penetration of the injected fluid into the mainstream at larger velocities causing the pressure to be lower downstream of the injection hole along the centerline which drives the hotter mainflow to these regions. The buffering effect of the injected flow is thus destroyed when the mass flow rates become higher. Again, this result cannot be conclusively extended to be true for all cases. The effect needs to studied in detail

for different injection angles and and variations in tubulence intensities, scale etc.

NEAR-TERM PLANS:

Through out this report many vistas of possible study have been suggested .Now that the procedure has been tested to satisfaction, the following further investigations are planned.

a) effects on the cooling effectiveness down stream and cross-stream with changes in:

i) injection angles.

ii) turbulence intensity and scales of injectant.

iii) different Reynolds number flows

iv) and many cross correlations of many of these parameters, (as we did see in this report the cooling effectiveness is insensitive to turbulence intensity for M=0.5 and 1.0).

b) study the flow pattern and its sensitivity to various parameters that have already been identified.

CONCLUSION:

The numerical solution procedure is successful in capturing the phenomenon of film-cooling. It can be seen that through these sensitivity studies we can establish the important parameters that effect the film cooling procedure.The results of such studies can aid an experimentalist to decide on design of the setup, and identify quantities that are important to be measured or deduced in course of the experiment. The numerical method can calculate all the variables that modeled at all locations in the domain and, the results, when confirmed through experiments will add to the body of information to a very large extent and thus provide a more compete picture of the flow scenario and more physical insight.

FUTURE PLANS

MORE FILM COOLING STUDIES:

More film cooling studies are being planned which include computing flow with more complex injection geometries, two rows of holes in a staggered configuration, more complex wall geometries viz curvature effects such as in the turbine blade geometries.

COMPLETE THREE DIMENSIONAL COMPUTATION:

This study is being planned to predict the horse-shoe vortex near the base of cylinder in the flow. This is being done as a preliminary study to investigate the flow near the base of a turbine blade. The effects on the film cooling of the blade geometries is also being planned.

E - HEAT TRANSFER NEAR THE BASE OF A PROTRUDING CYLINDER

To model heat transfer at the leading edge of a turbine blade, in particular in the three dimensional region near the end-wall, a basic understing of the flow and heat transfer of the region is needed. Heat transfer in this area, both on the turbine and on the end-wall, is influenced by the presence of horse-shoe vortex, inner vortices, and the separation and reattachment that may follow. To document this influence a basic study to investigate flow and heat transfer around geometrically simple objects, such as a circular and rectangular cylinders protruding from a plate, is undertaken. Naphthalene sublimation is used to measure local mass (heat) transfer coefficient on the cylinder and its base plate. Results of the study with the circular cylinder are already published. Measurements using a rectangular cylinder are underway and few sample results are presented here in.

A typical distribution of the heat transfer coefficient on the front face of a rectangular cylinder is shown on Fig. E-1. On Figure E-2 contours of heat transfer coefficient on the front face and on the end-wall are shown. These data show that the inner vortex causes very high heat transfer near the junction of cylinder and its end plate. To better explain the peaks of heat transfer in this region, a closer examination of these data together with a flow visualization study are underway.

The influence of approaching mainstream velocity and boundary layer thickness is also investigated. Effect of the change in boundary layer thickness, brought about by changing the trip-wire tdiameter, is presented on Figs. E-3 and E-4. These figures show that thickening boundary layer increases heat transfer on the front face of the cylinder near the end-wall; at locations farther up and on side faces its effect is practically negligible. On the rear face, however, the boundary layer effect extends further up along the cylinder. Boundary layer thickness affects mass transfer from the end-wall only in the wake behind the cylinder, Fig. E-4. The effect of changing the angle of attack on local and average heat transfer are also

considered. The local effect swere presented previously; here the effect on average heat transfer around the cylinder in the two dimensional region is depicted, Fig. E-5.

Currently, a detailed visualization study is planned to complement the heat transfer data to provide insight on the fluid flow and verification of the existence of inner vortices and their behavior.

F. THE TWO-HALF-BLADE CASCADE TEST

INTRODUCTION

In this study, the streamwise variation of surface curvature and static pressure gradient as well as the three-dimensionality of the blade/end-wall region of an actual engine airfoil are simulated in a large-scale cascade section. When completed, this facility will allow detailed measurements of the flow within a cascade with better resolution than had been made in earlier, smaller cascades.

Anticipated studies within this facility include detailed measurements of the flow in the end-wall region and testing of schemes for controlling the passage vortex. Later portions of the project may include detailed hydrodynamic studies of film cooling flow. The three-dimensional end-wall region holds a very complicated flow consisting of boundary layers, large-scale vorticies and gross secondary flows. This complexity and the small scale of actual-size or near-actual-size airfoils prevent one from probing the flow in detail. Such measurements supplement the detailed wall measurements, taken as an earlier portion of this study, and the numerical predictions of this flow. This scaled-up test facility is, thus, of great value. As more is learned about the interaction of cross-stream pressure gradients, vorticies, and boundary layer flow, more can be done toward numerically modeling the flow. Then, the experimental facility and the numerical program can, in concert, be used to devise means to manage the flow in this very important region of the gas turbine.

The study is to begin with the construction of the large-scale single-stage, two-surface cascade shown on Fig. F-1. Appropriate flow control will be applied to locate the stagnation points at the appropriate leading edge positions on the airfoil surfaces and the walls will be positioned such that the actual streamwise pressure gradients are simulated. Measurements to be made include the following:

1). Mean and fluctuating components of the three velocity components. A triple-wire probe will be used.

2). Scales in the flow. Two hot-wires separated in the streamwise, cross-stream, and spanwise directions will be used. Autocorrelations using a single wire will also be performed.

3). Wall shear stresses. A special hot-wire probe for near-wall measurements is available for this purpose.

Because the flow is rich in coherent vorticies, instrumentation for measuring vorticity will be sought and, if found, implemented. Vorticity probes have been under development by various researchers for several decades. No one technique is universally applicable, however.

Experience from the extensive measurement program employed in the curved-wall recovery test will be available for this test.

PRESENT STATUS OF WORK

The flow delivery section to be used in this study is presently in-house, the remaining steps in installation will be completed in the next few weeks. Design of an unheated cascade section to verify the feasibility of the test is now underway

REFERENCES

Blair, M.F., and Bennett, J.C., (1984) Hot-wire measurements of velocity and temperature fluctuations in a heated turbulent boundary layer, 29th-ASME International Gas Turbine Conference, Amsterdam.

Gibson, M.M., and Verriopoulos, C.A., (1984) Turbulent boundary layer on a mildly curved convex surface, Exp. in Fluids 2, Springer-Verlag, pp. 73-80.

Goldstein, R.J., Eckert, E. R. G. Ericksen,V. L., and Ramsey, J.W., (1970) Film cooling following injection through inclined circular tubes., Israel J. of Technology, Vol.8, p. 145.

Hishida M., and Nagano Y., (1978) Simultaneous Measurements of Velocity and Temperature in Nonisothermal Flows, J. Heat Transfer, Vol. 100, pp. 340-345.

Jabbari, M.Y., and Goldstein, R.J., (1978) Adiabatic Wall temperature and heat transfer downstream of injection through two row of holes, Eng.of Power, Vol. 100, No.2, pp 303-307.

Kadotani, K., and Goldstein, R.J., (1979) Effect of mainstream variables on jets issuing from a row of inclined round holes , Eng.of Power, Vol. 101, No.2, pp 298-304.

Kim, J. and Simon, T.W. (1988) Measurements of the turbulent transport of heat and momentum in convexly curved boundary layers: Effects of curvature, recovery, and free-stream turbulence, J. of Turbomachinery, Vol. 110, No. 1, pp. 80-87.

Patankar, S.V. (1980) Numerical Heat Transfer and Fluid Flow, Hemisphere Pub. Co.

Patankar, S.V., and Spalding, D.B., (1972a) A calculation procedure for heat , mass and momentum transfer in three dimensional parabolic flows , Int. J. Heat Mass Transfer, Vol. 15, No. 2, p. 1787.

Rodi, W. (1980) Turbulence Models and their Applications in Hydraulics, Book publication of Int. Ass. for Hydraulic Research, Delft, The Netherlands.

Wang, T., and Simon, T.W., (1987) Heat transfer and fluid mechanics measurements in transitional boundary layers on convex-curved surfaces, ASME J. of Turbomachinery, Vol. 109, No. 3, pp. 443-452.

You, S.M., Simon, T.W., and Kim, J., (1986a) Boundary layer heat transfer and fluid mechanics measurements on a mildly-curved convex wall, Proc. Eighth Int. Heat Transfer Conf., Vol. 3, pp. 1089-1094.

You, S.M., Simon, T.W., and Kim, J., (1986b) Free-stream turbulence effects on convex-curved turbulent boundary layers, ASME Paper No. 86-WA/HT-46.

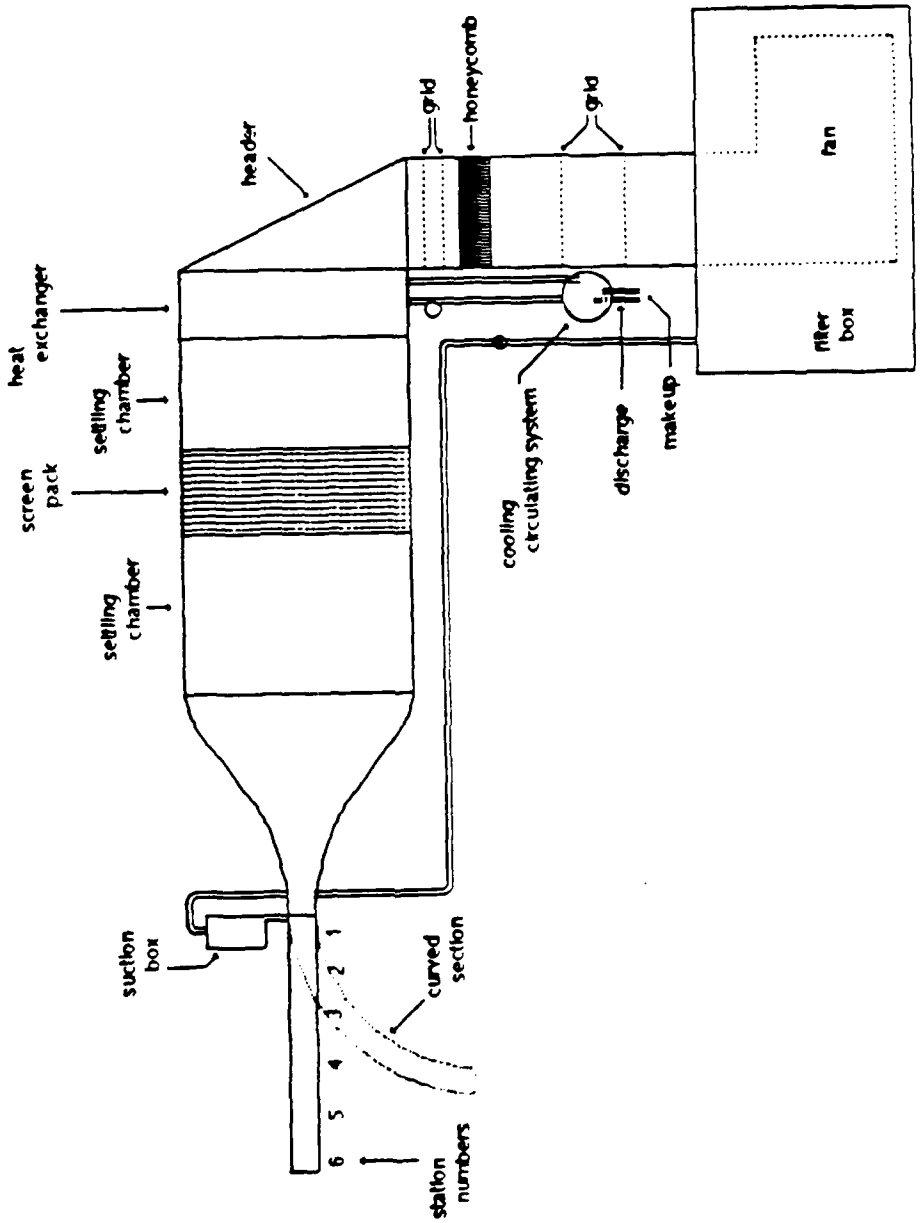

Fig. A-1 -- Schematic of test facility.

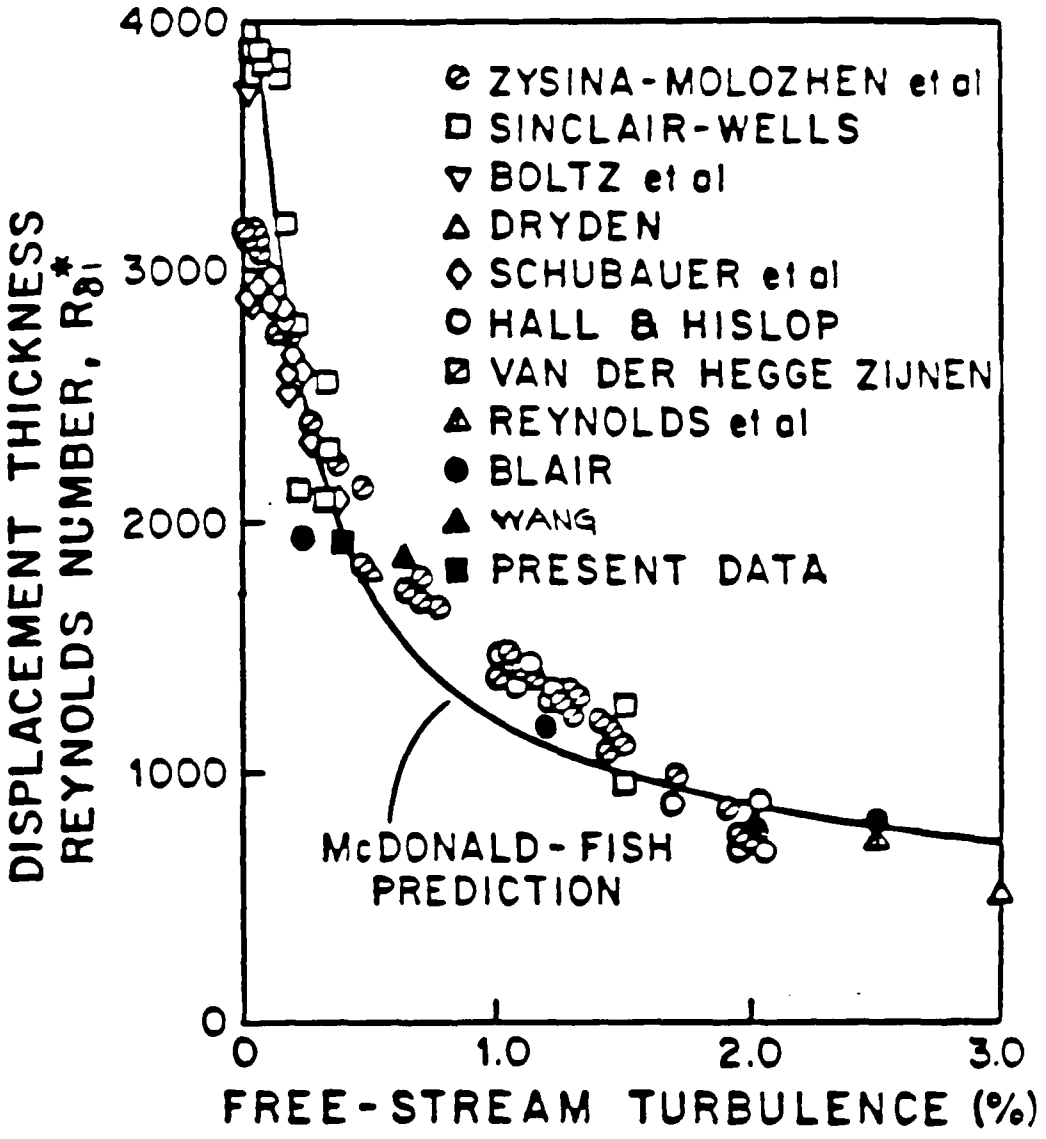

Fig. A-2 -- Transition start location. Comparison with other researchers

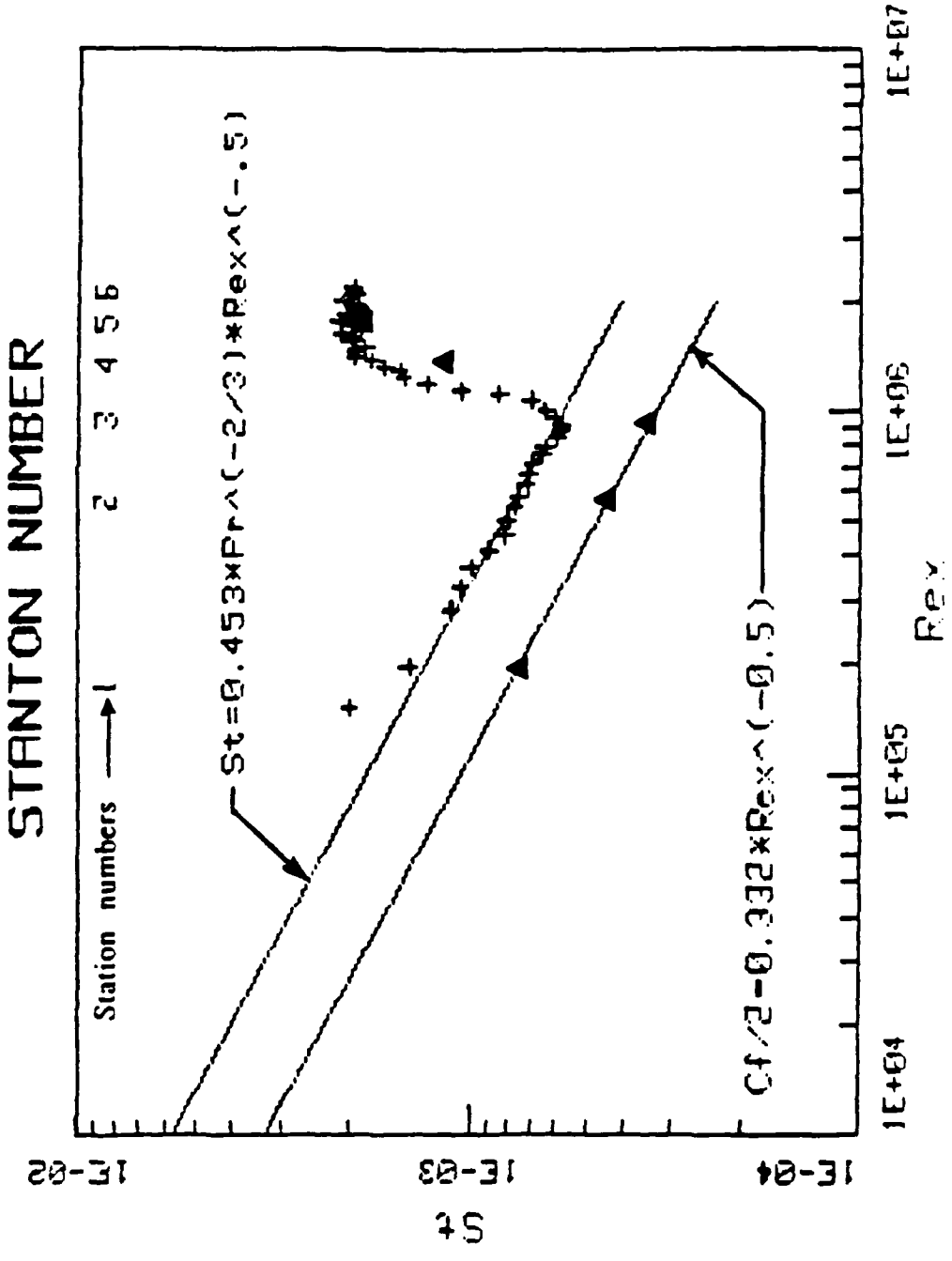

Fig. A-3 -- Stanton number and skin friction variation along the wall.

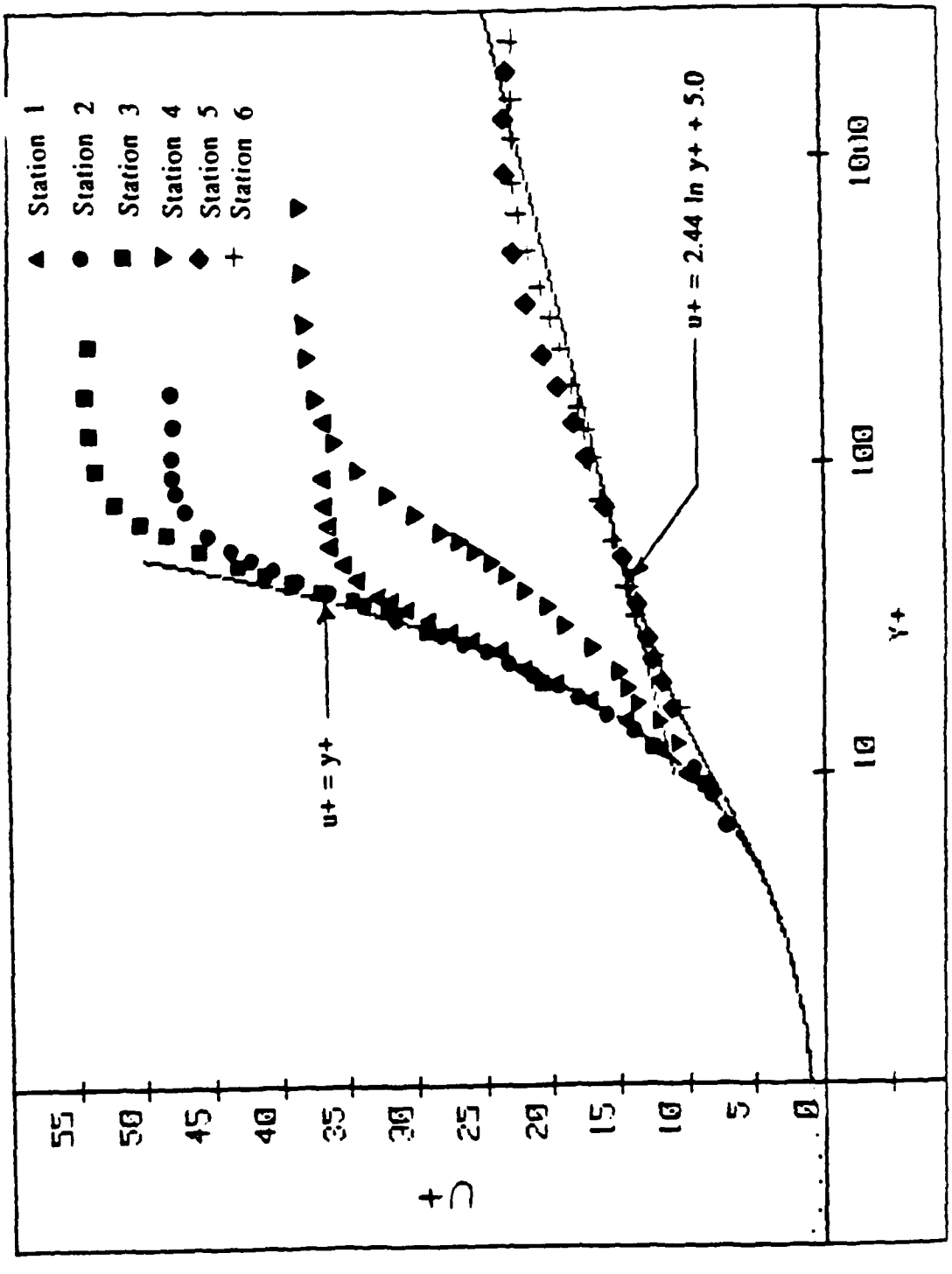

Fig. A-4 -- Non-dimensional velocity profiles.

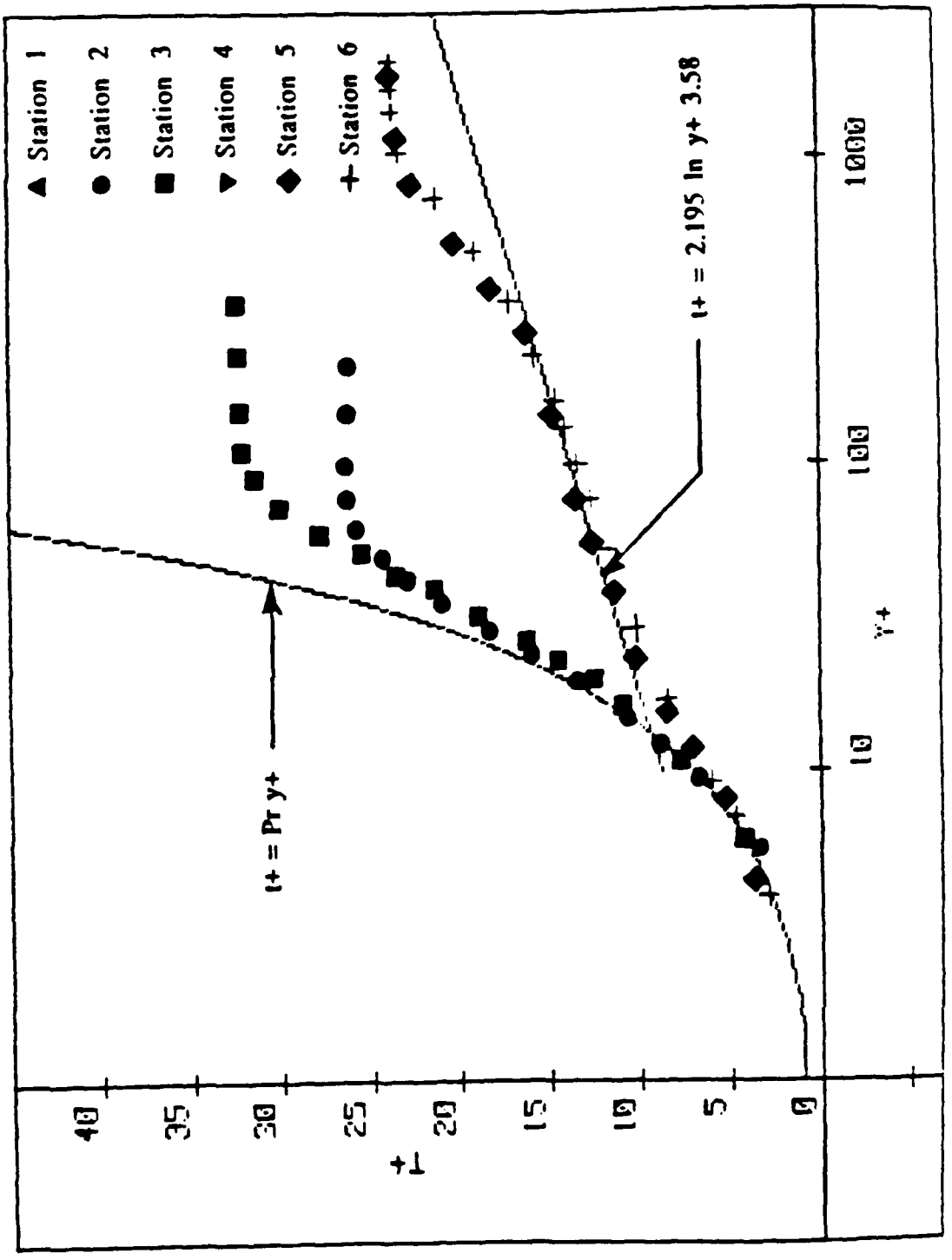

Fig. A-5 -- Non-dimensional temperature profiles.

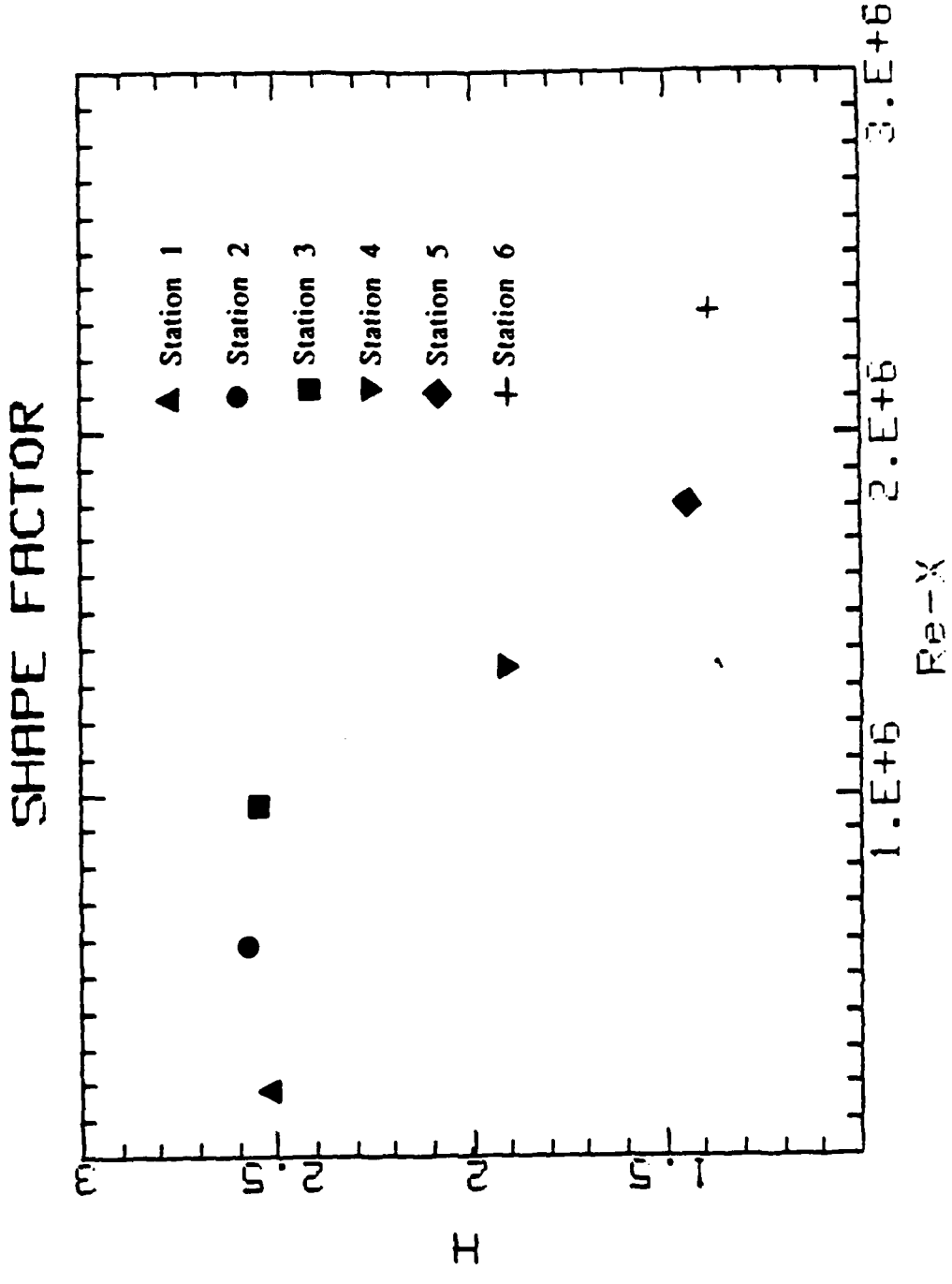

Fig. A-6 -- Shape factor variation through transition.

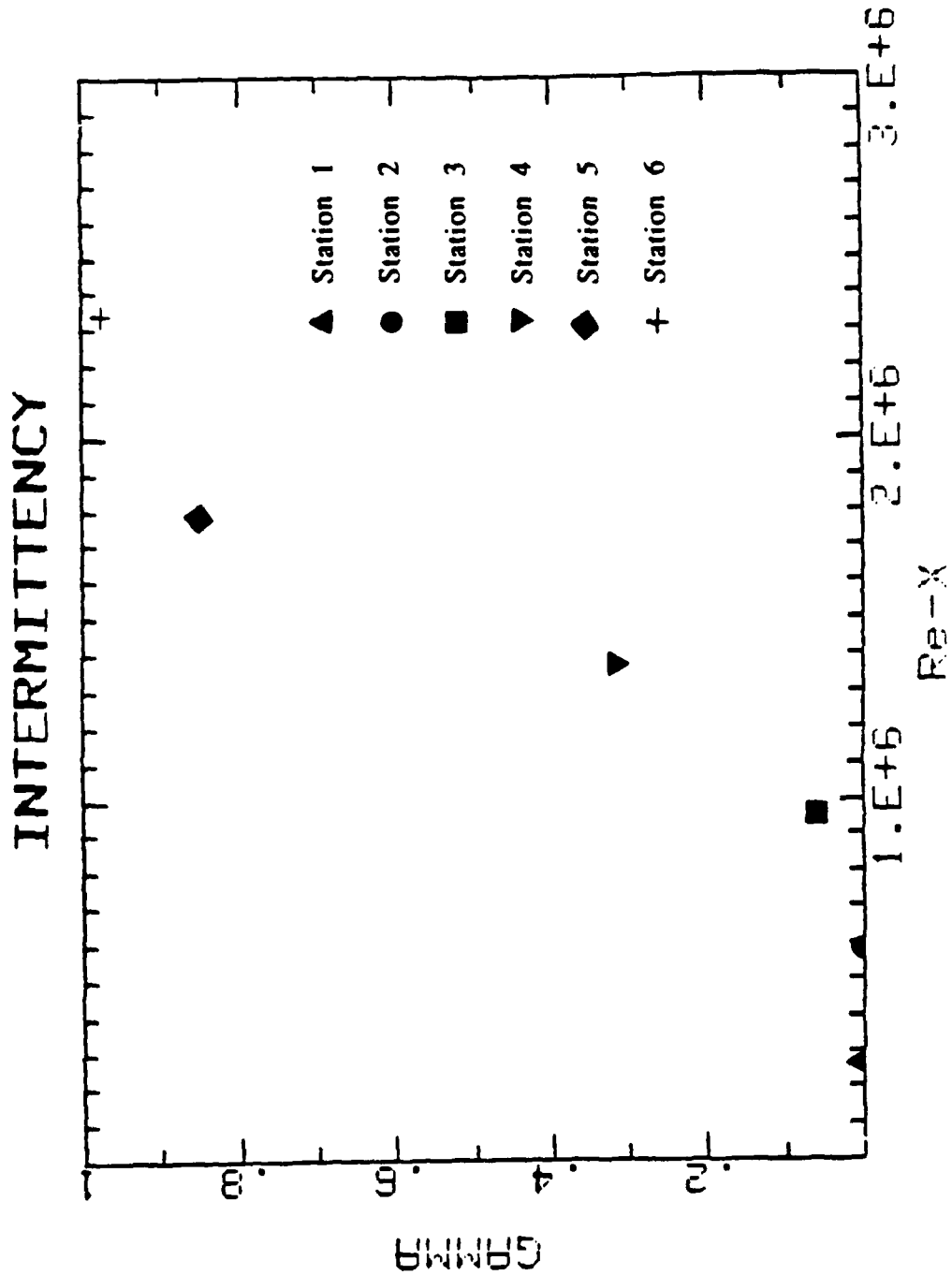

Fig. A-7 -- Intermittency along the wall.

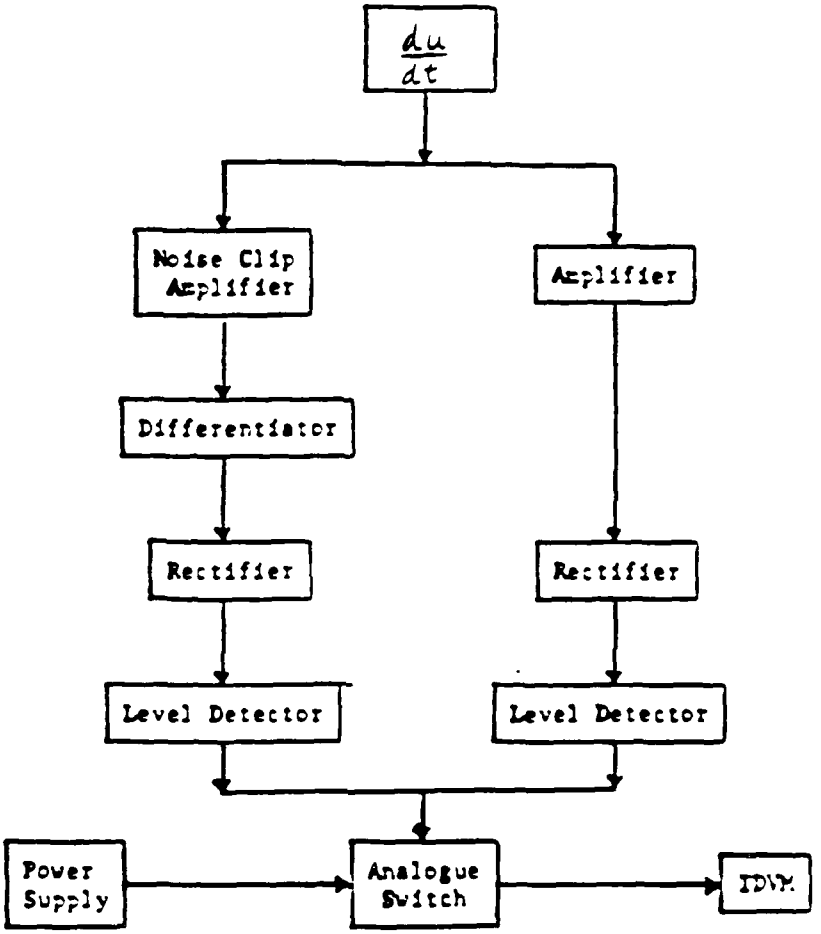

Fig. A-8 -- Schematic of intermittency circuit.

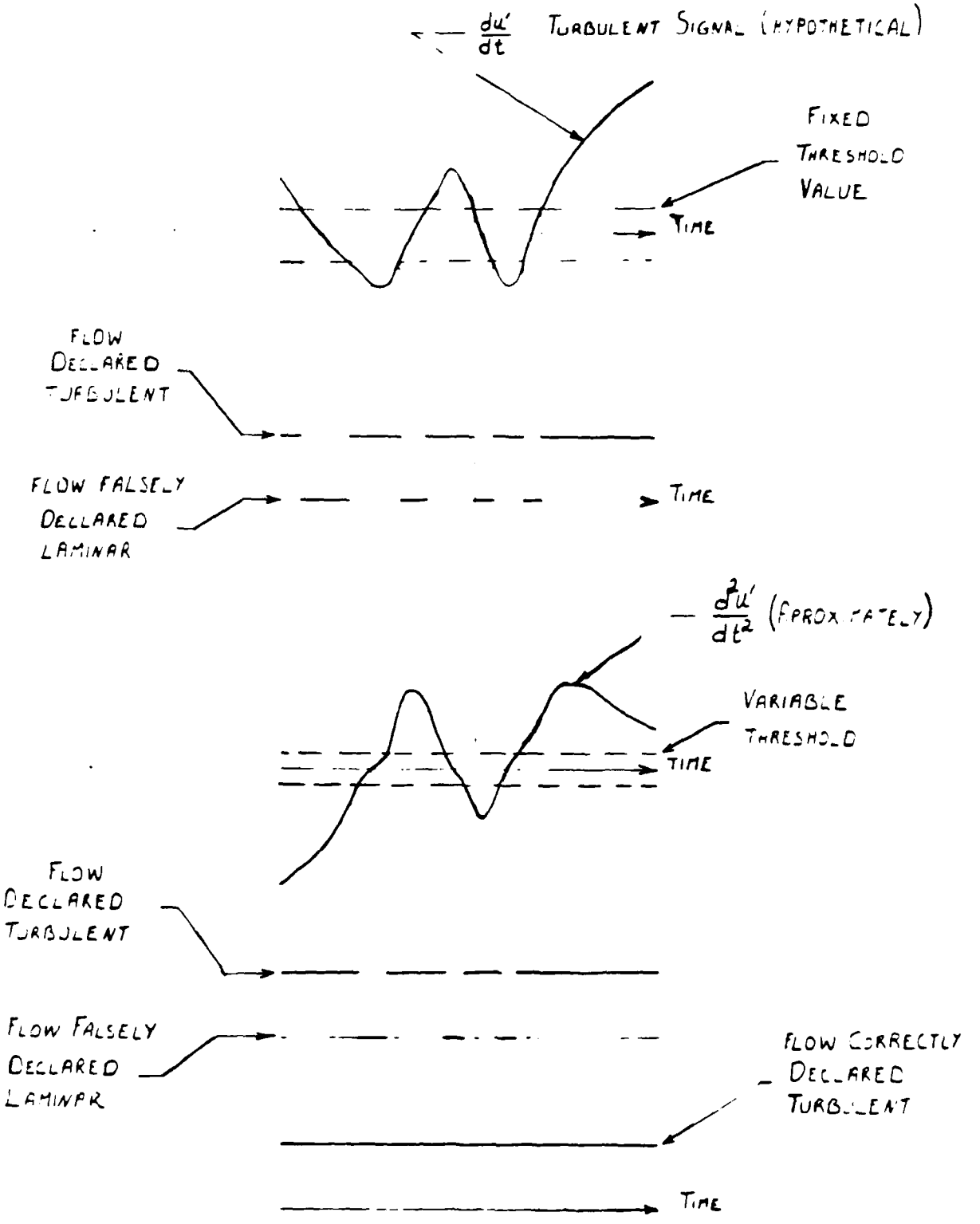

Fig A-9 Avoiding the Problem of Zero Crossing

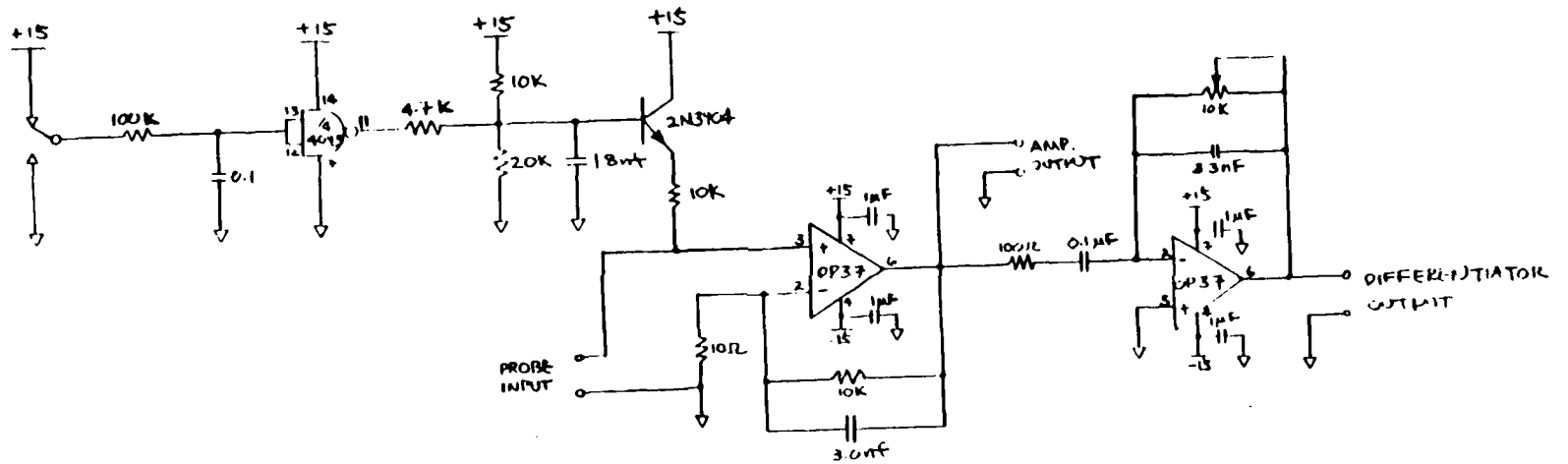

Fig. A-10 -- Circuit for Driving Cold-wire

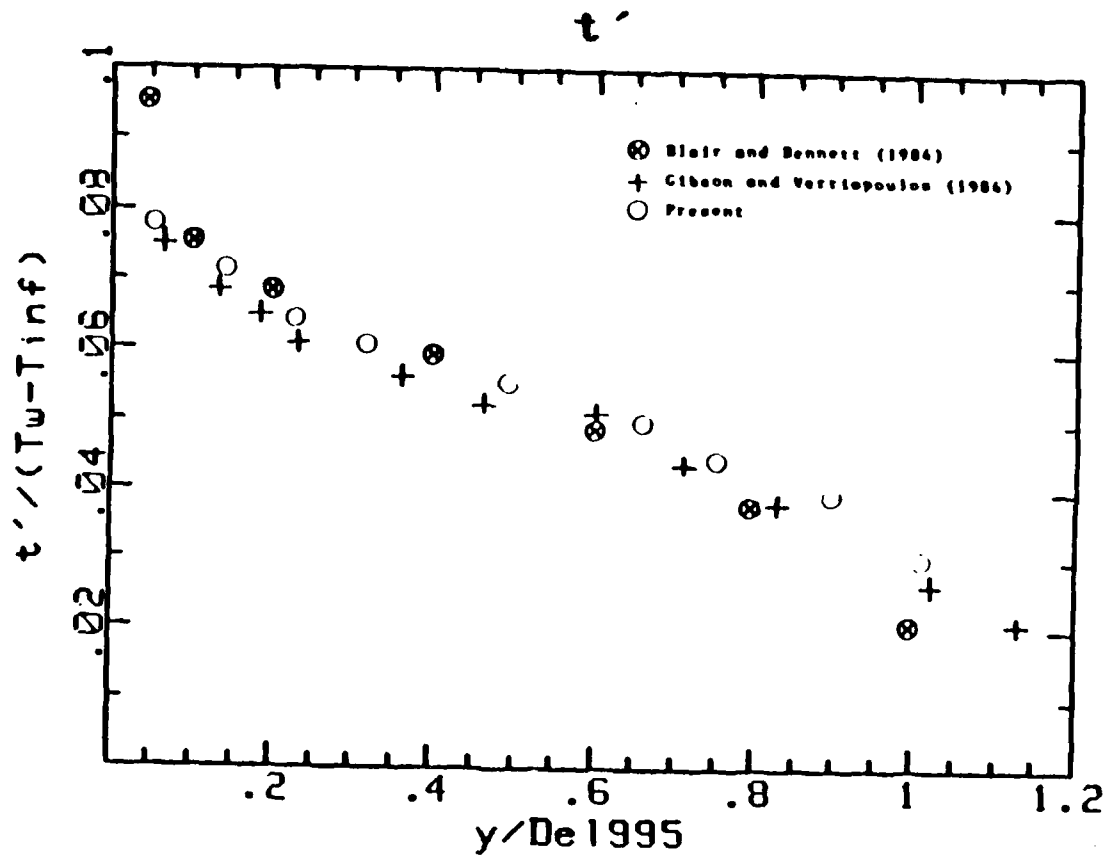

Fig. A-11 -- Profile of the Fluctuating Temperature in a Turbulent Boundary Layer

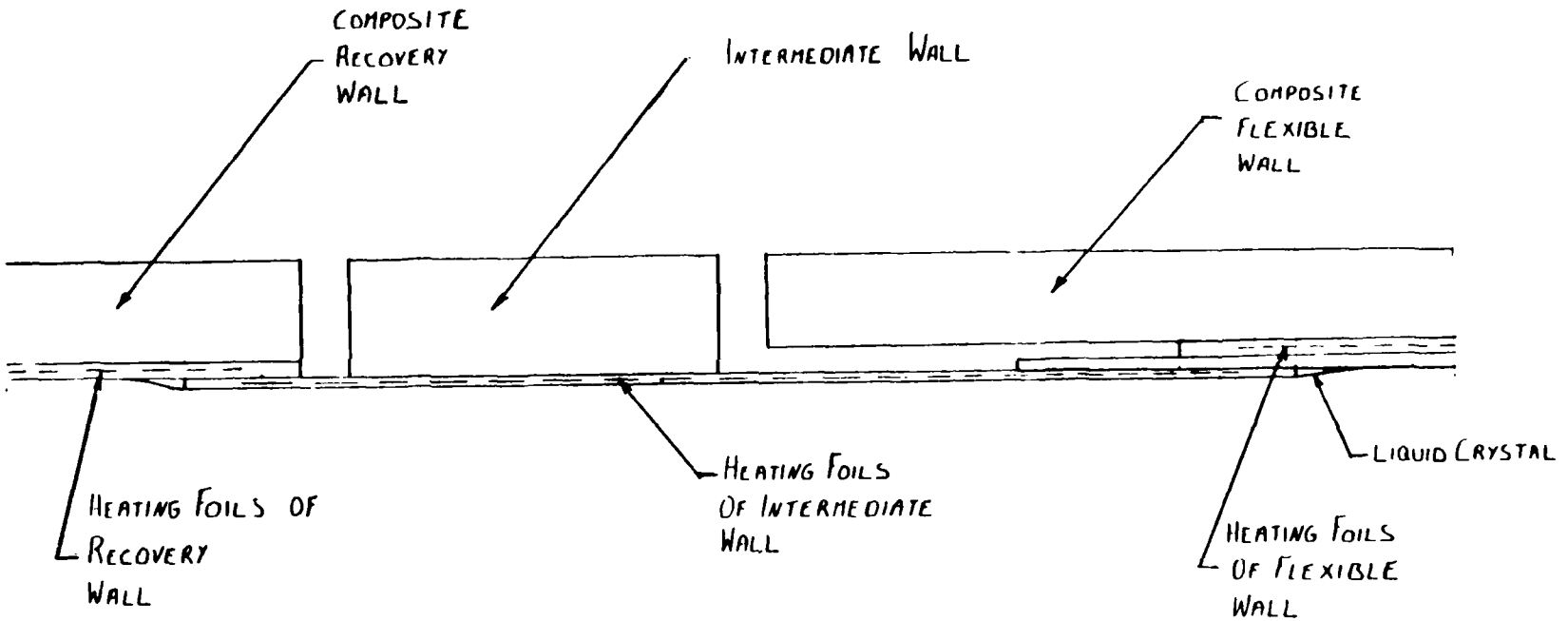

FIG A-12 INSTALLATION OF THE RECOVERY WALL
(APPROXIMATE SCALE 1.5)

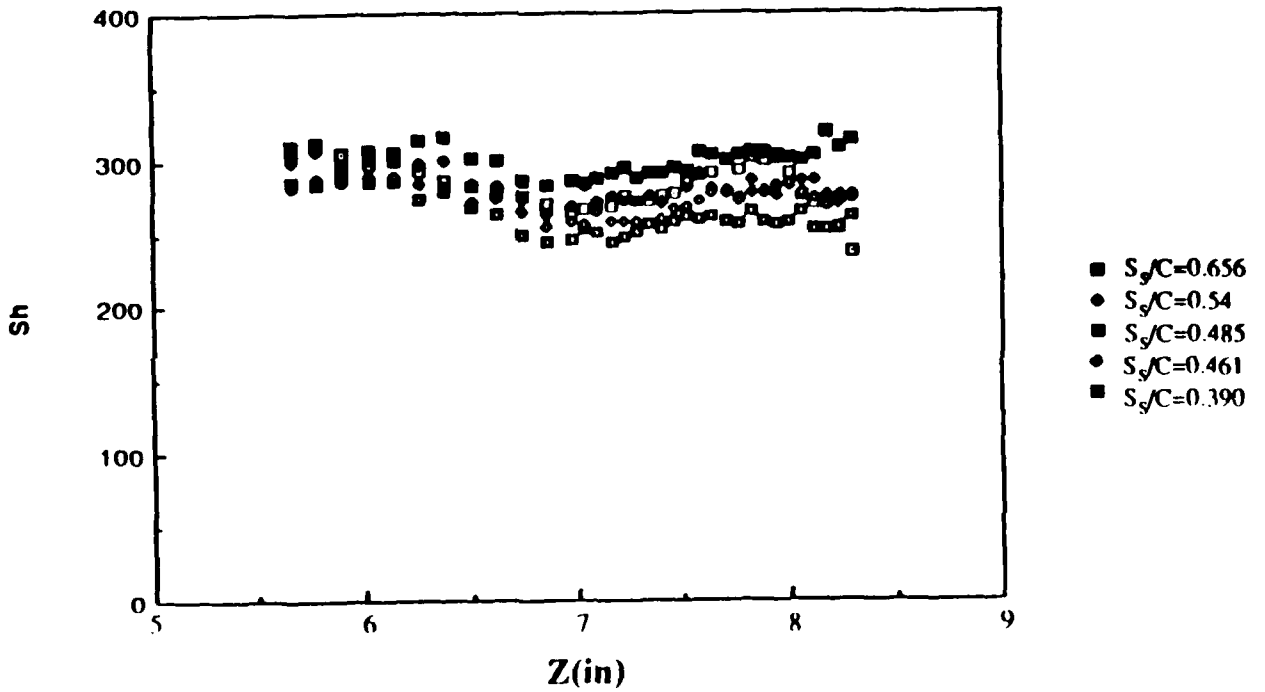

Figure B 1 - Spanwise distribution of local Sherwood number on the convex surface at five curvilinear locatiions

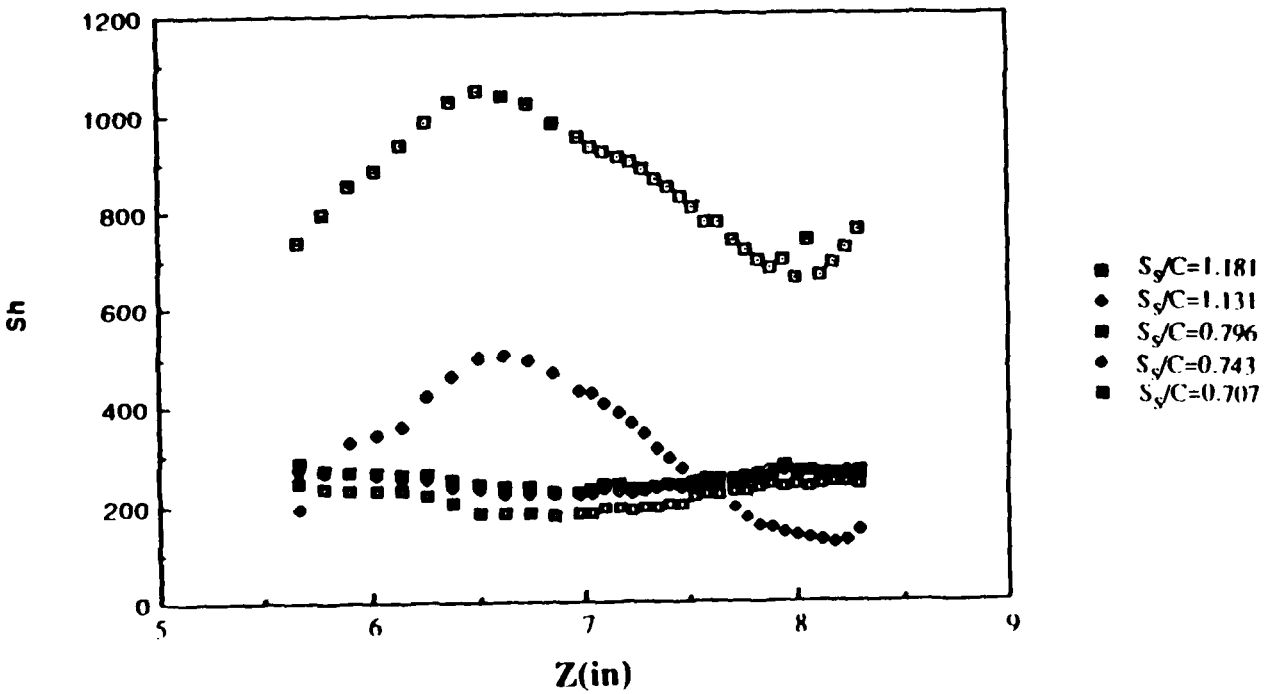

Figure B 2 - Spanwise distribution of local Sherwood number on the convex surface at five curvilinear locations

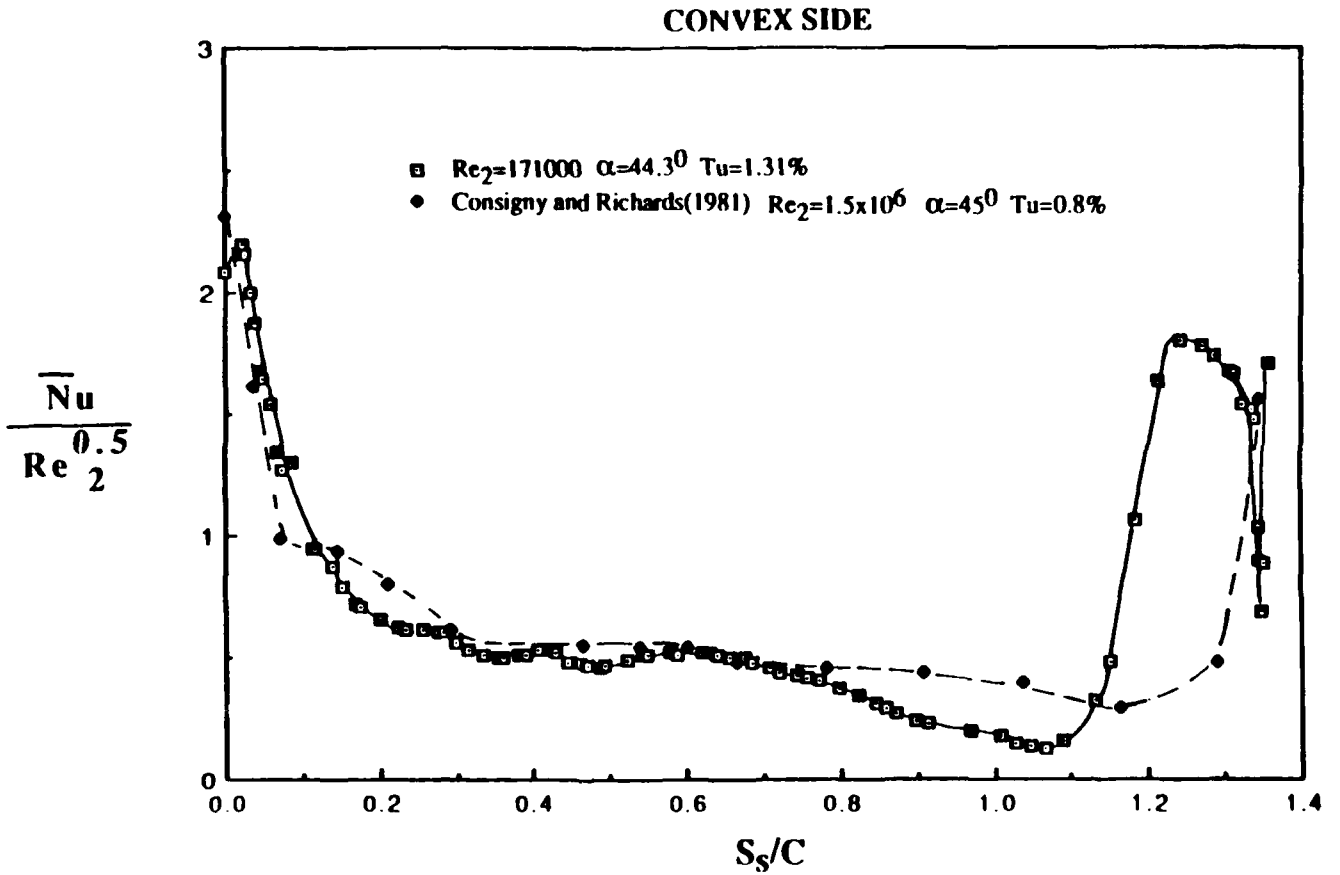

Figure B 3 - A comparison of curvilinear distribution of average Nusselt number on the convex surface between the present study and the study by Consigny and Richards (1981)

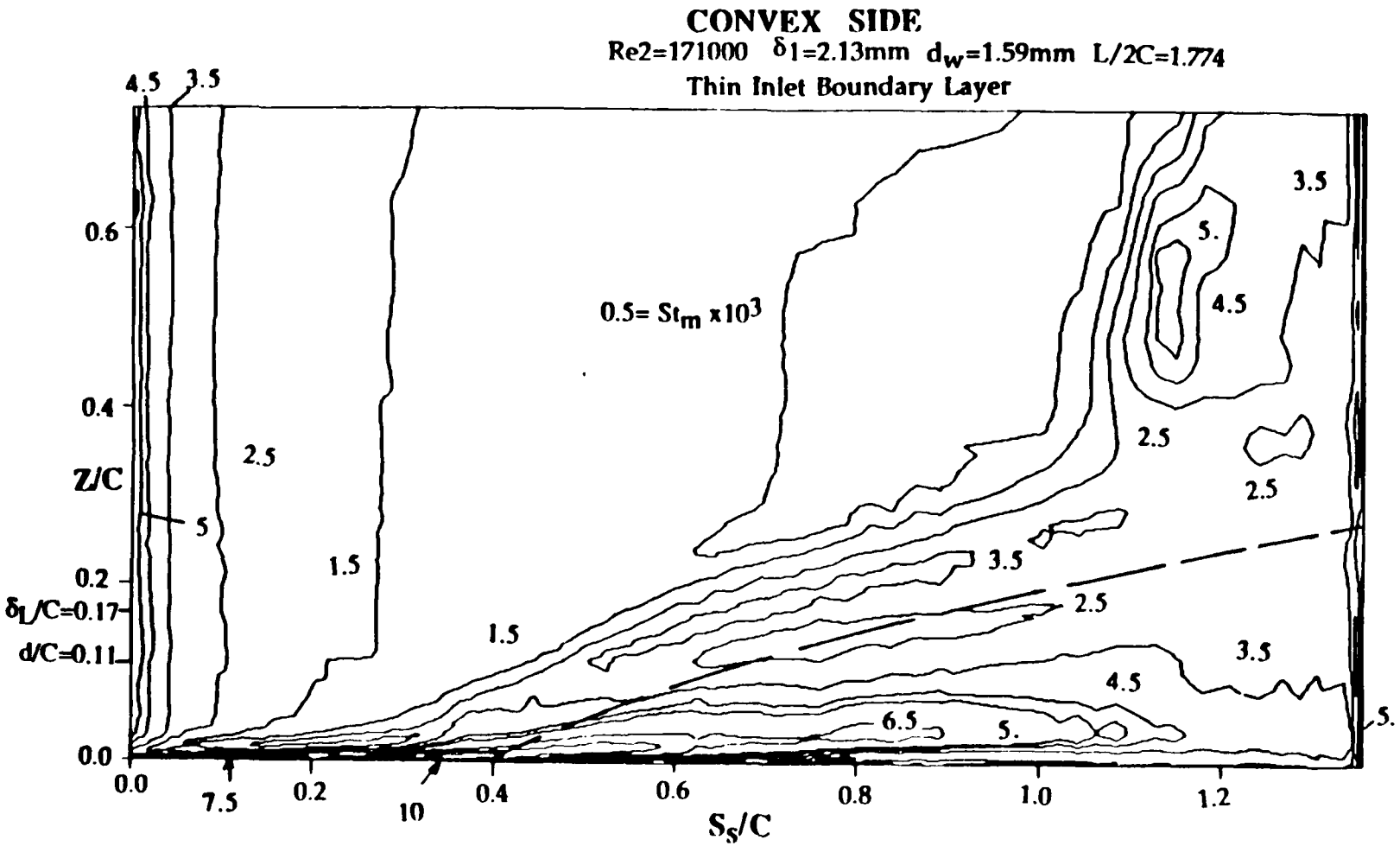

Figure B 4 - Convex surface Staton number contours at δ1 = 2.13mm

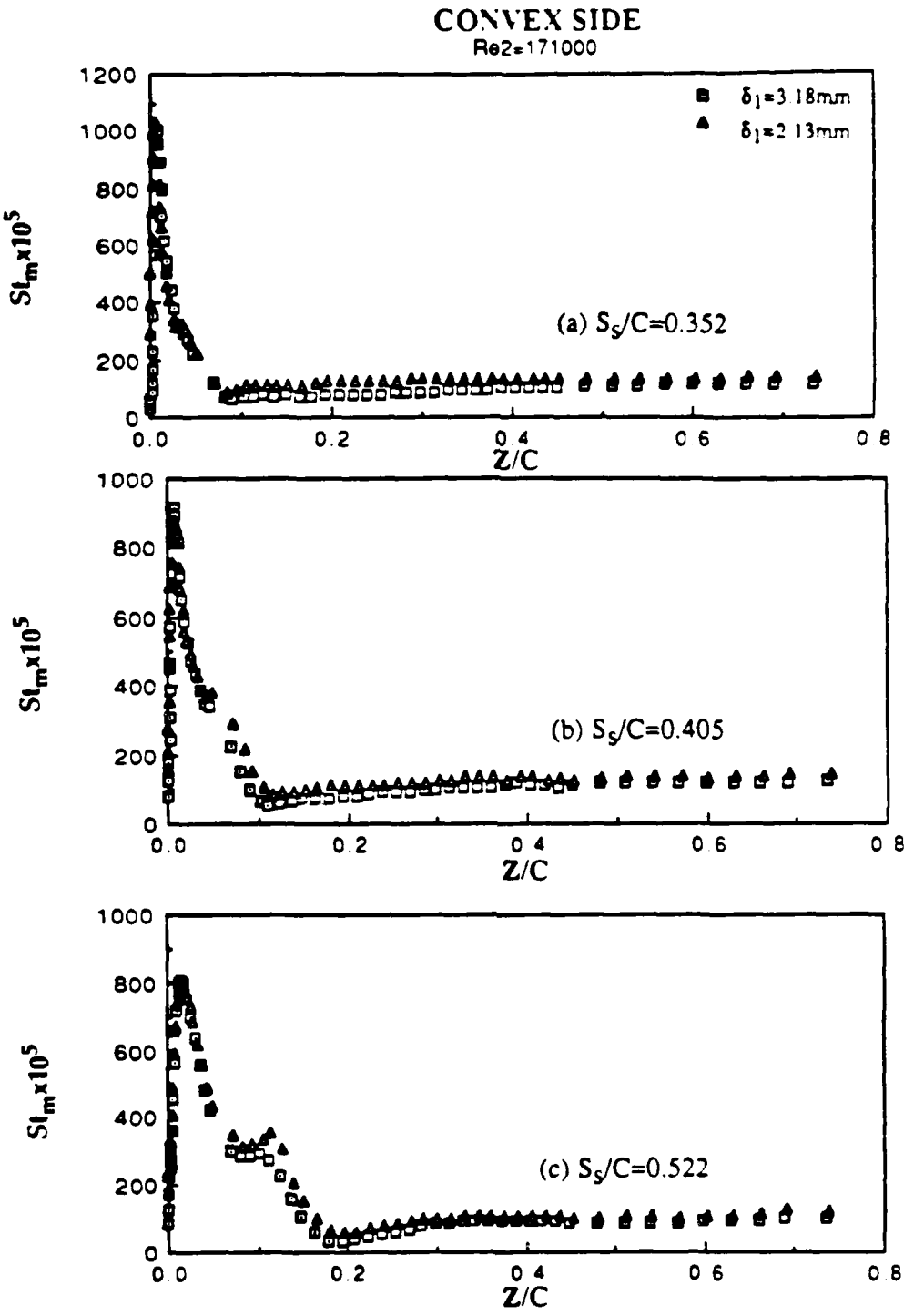

Figure B 5 - A comparison of spanwise distribution of local Stanton number on the convex surface at selected curvilinear locations between cases of two different displacement thicknesses.

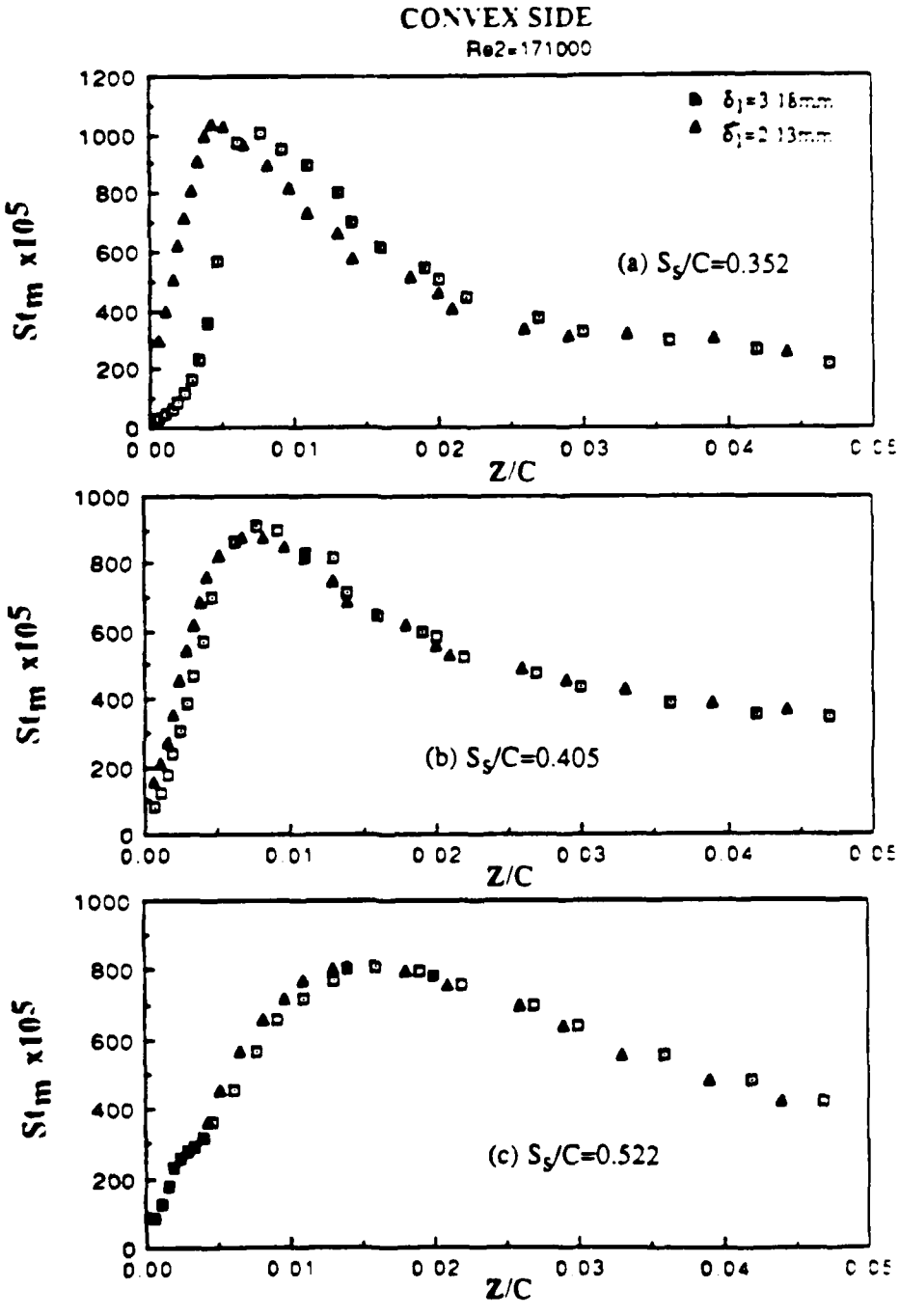

Figure B 6 - Enlargement of Figure B 5 in the region near the endwall

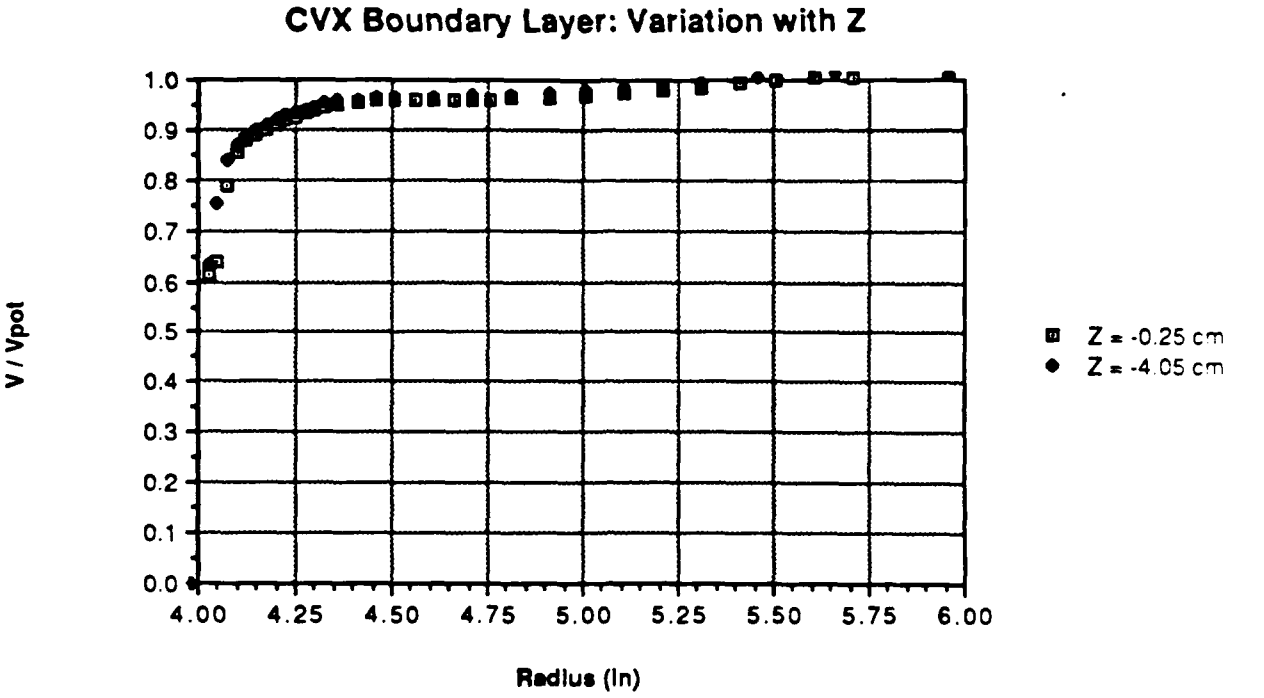

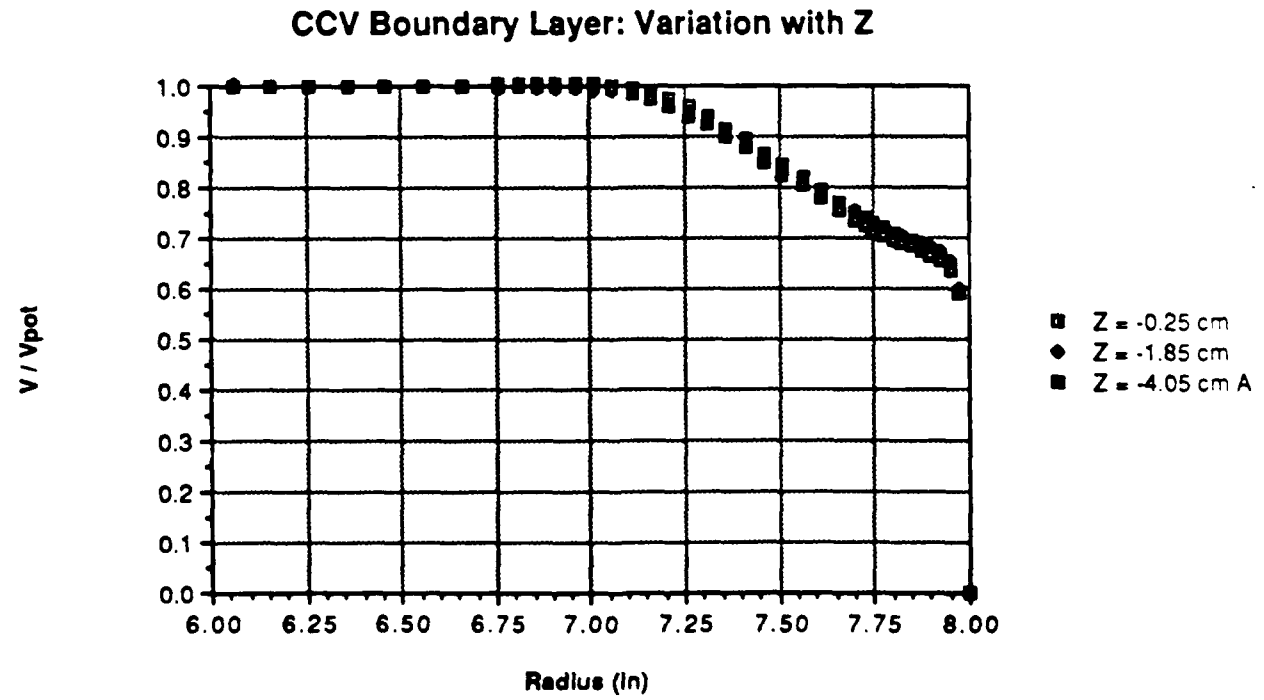

Figure C 1 - Boundary layer velocity distribution along the wall span

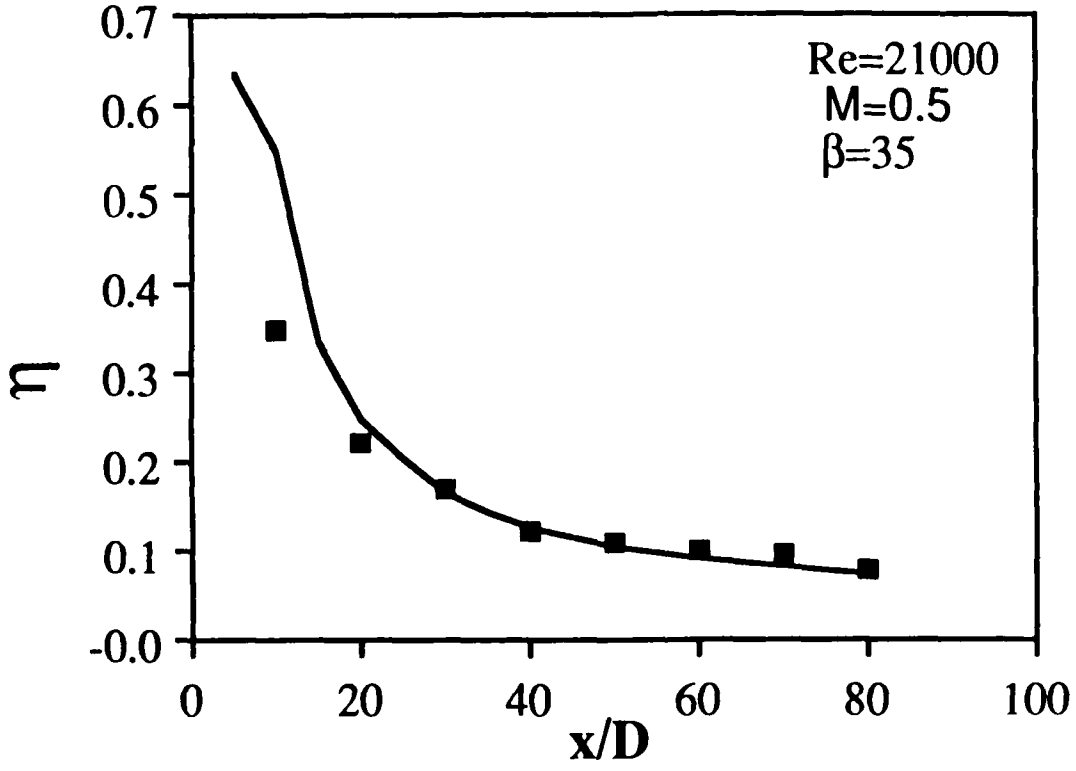

D-1. Comparison of experimental and computed results

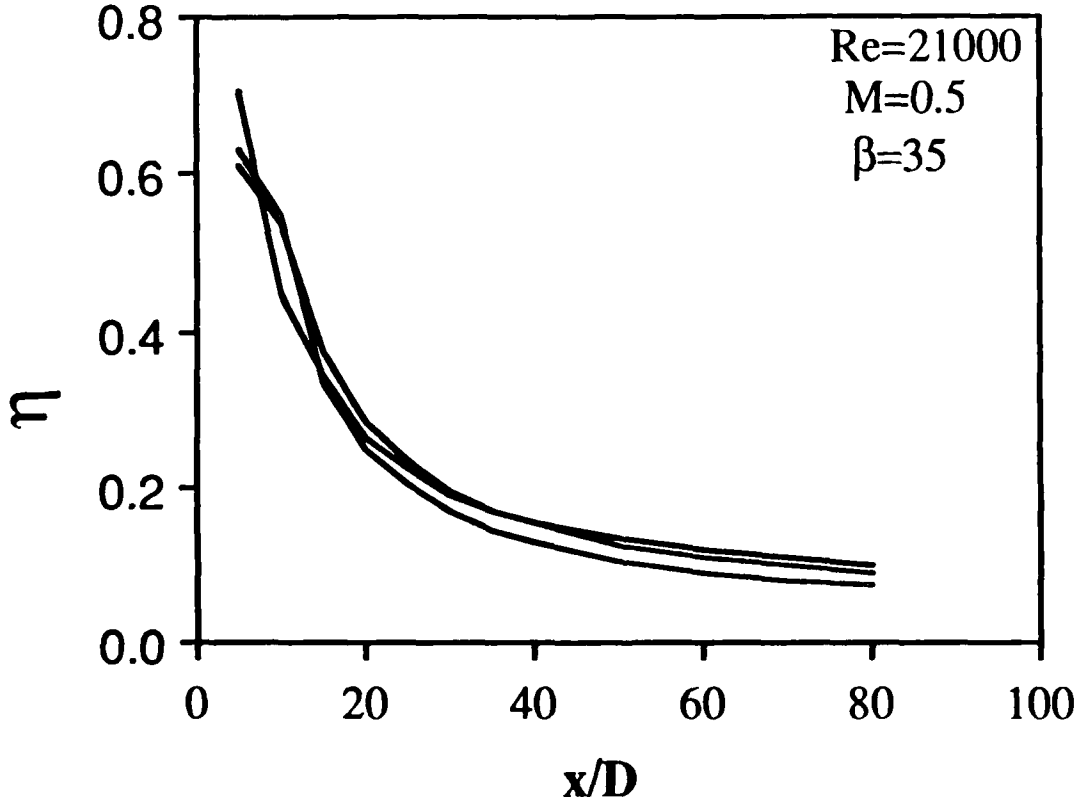

D-2. Sensitivity of cooling effectiveness due to turbulence intensity

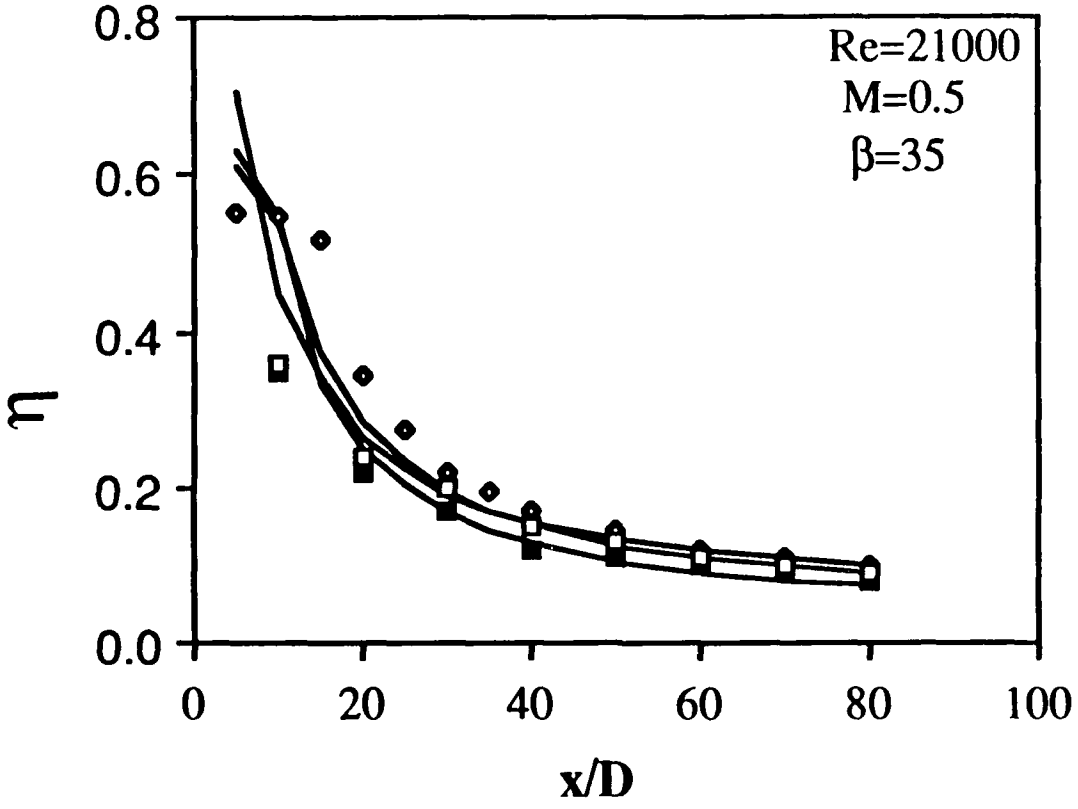

D-3. Experimental and computed results for the sensitivity of cooling effectiveness to turbulence intensity

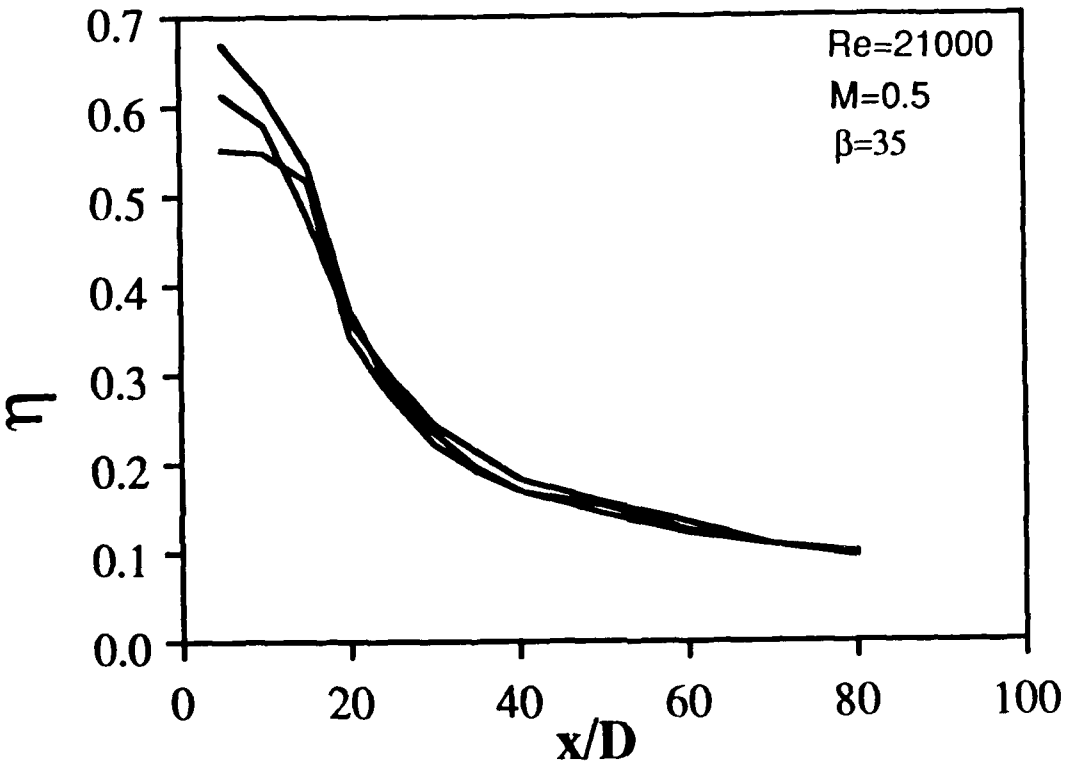

D-4. Sensitivity of cooling effectiveness to free-stream dissipation

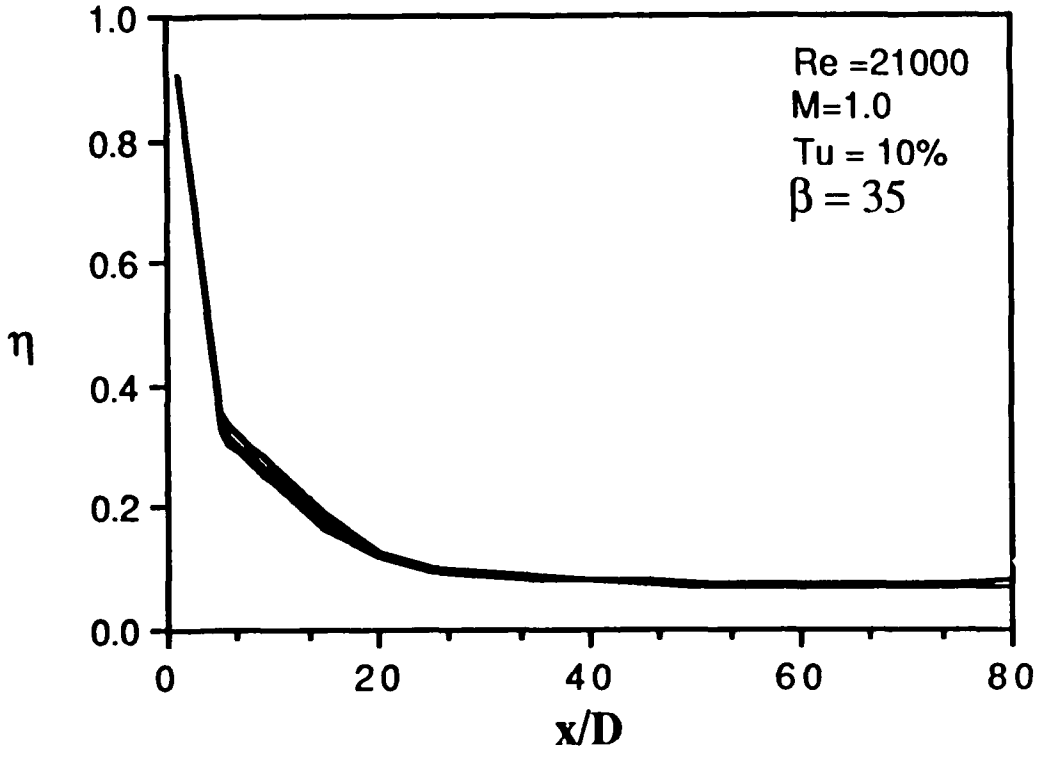

D-5. Effect of Turbulence scale (dissipation) on cooling effectiveness

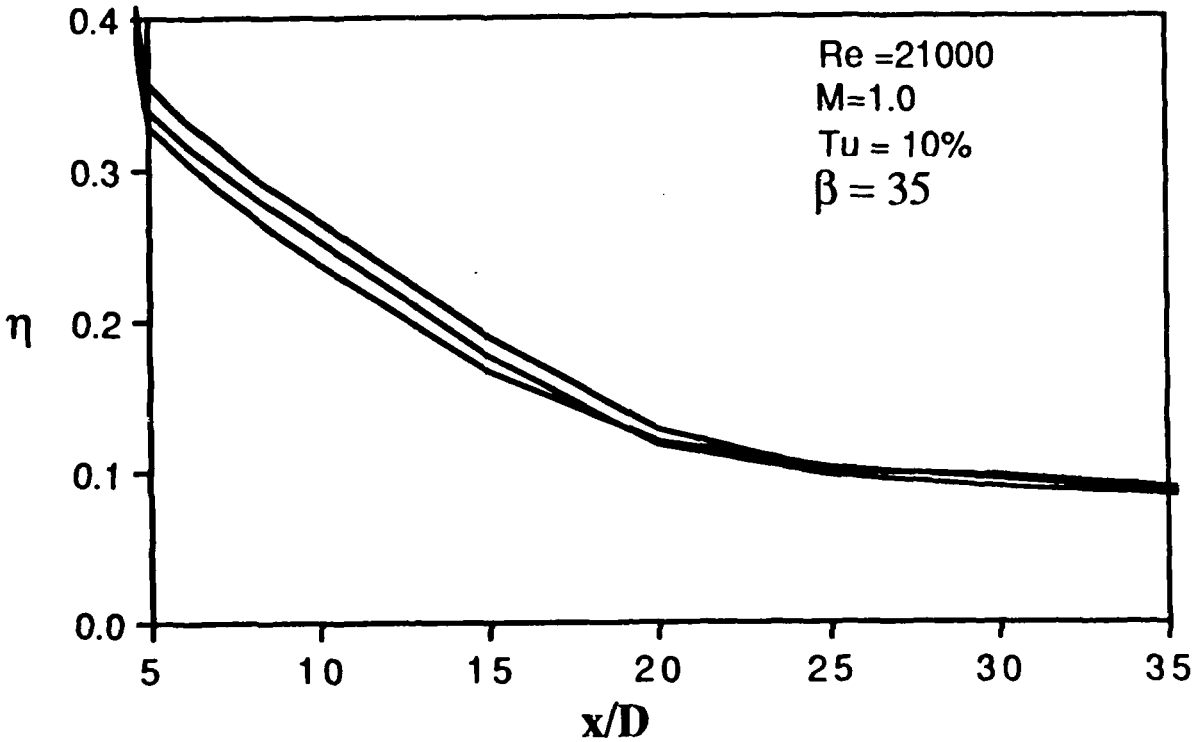

D-6. Effect of Turbulence scale (dissipation) on cooling effectiveness
(magnified view)

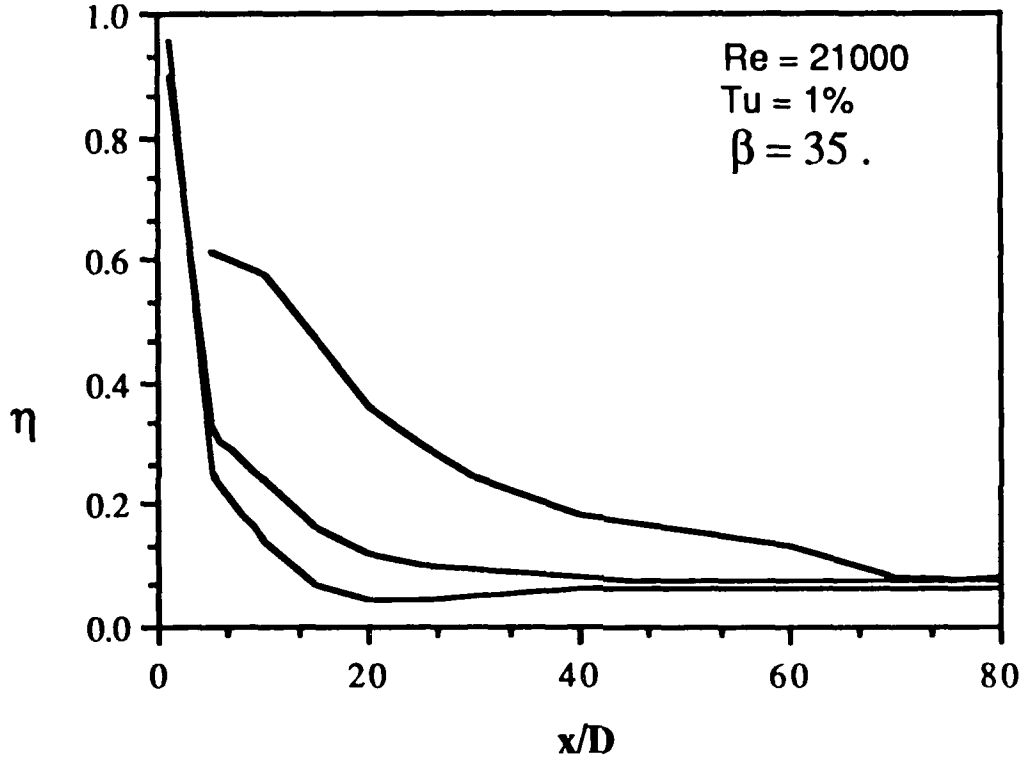

D-7. Effect of injection flow rate (M) on cooling effectiveness

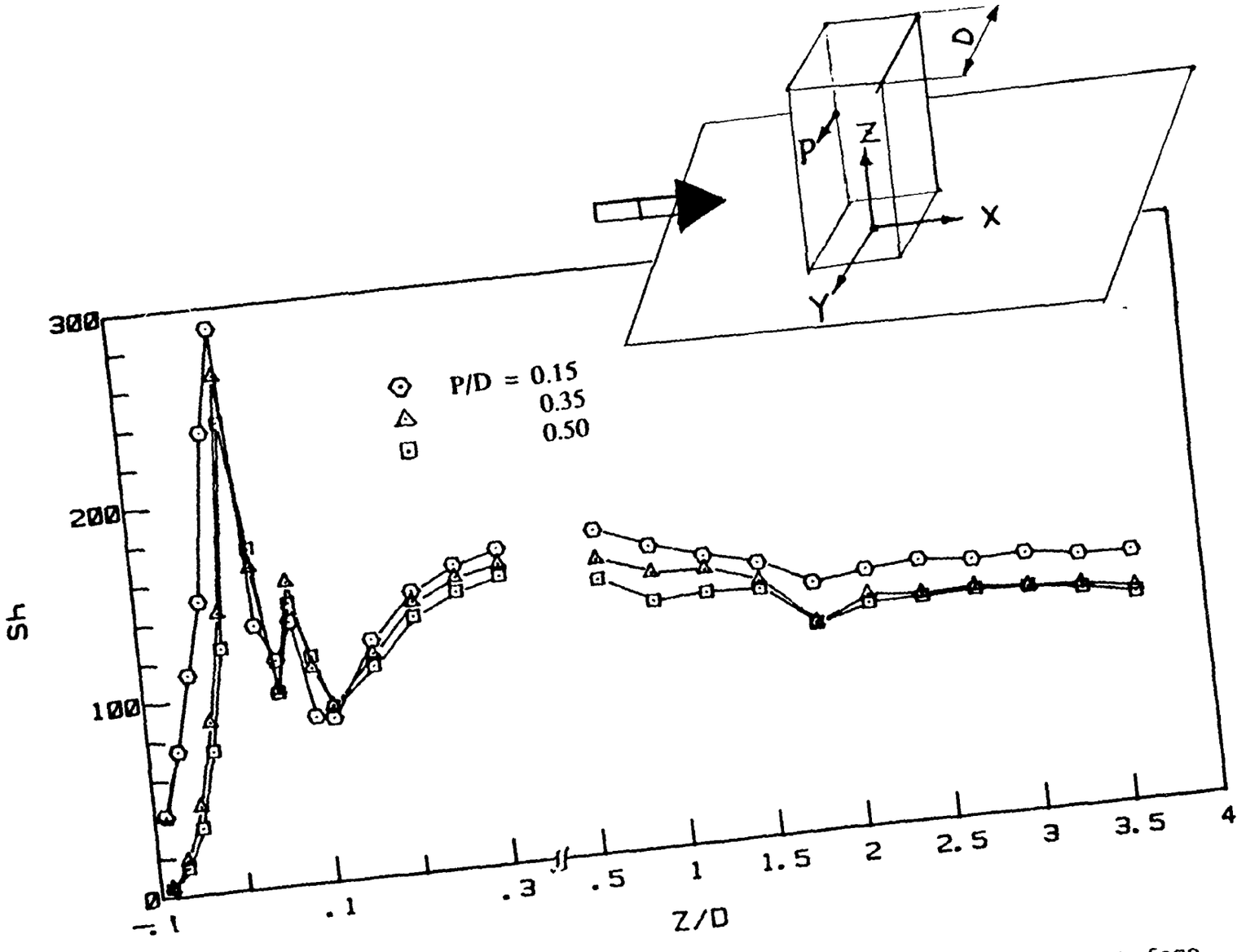

Figure E 1 - Variation of Sherwood number along the cylinder - front face
(Re - 18600, alpha = 0)

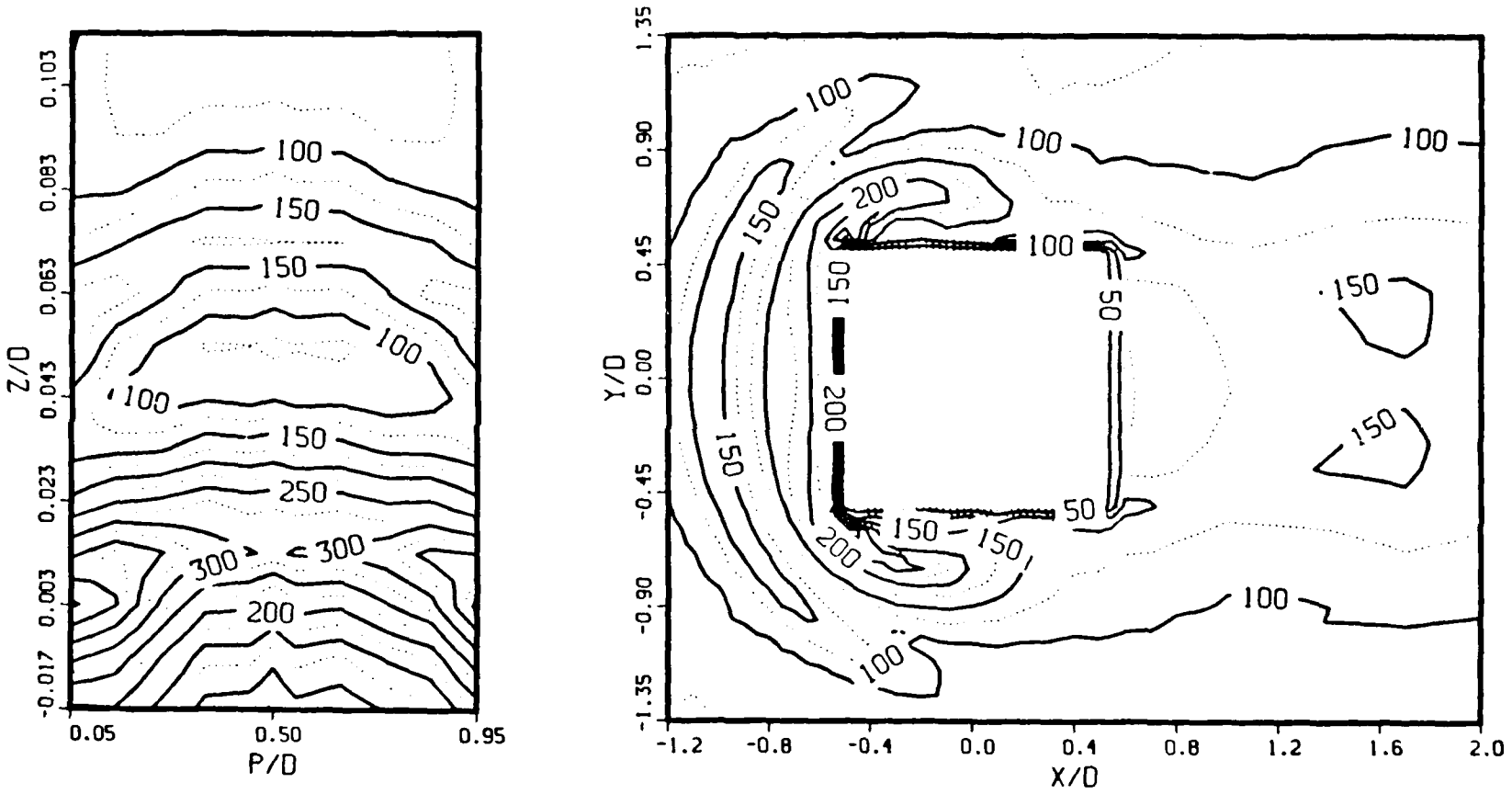

Figure E 2 - Contour of Sherwood number on the cylinder (left) and the plate (right) (Re - 18900)

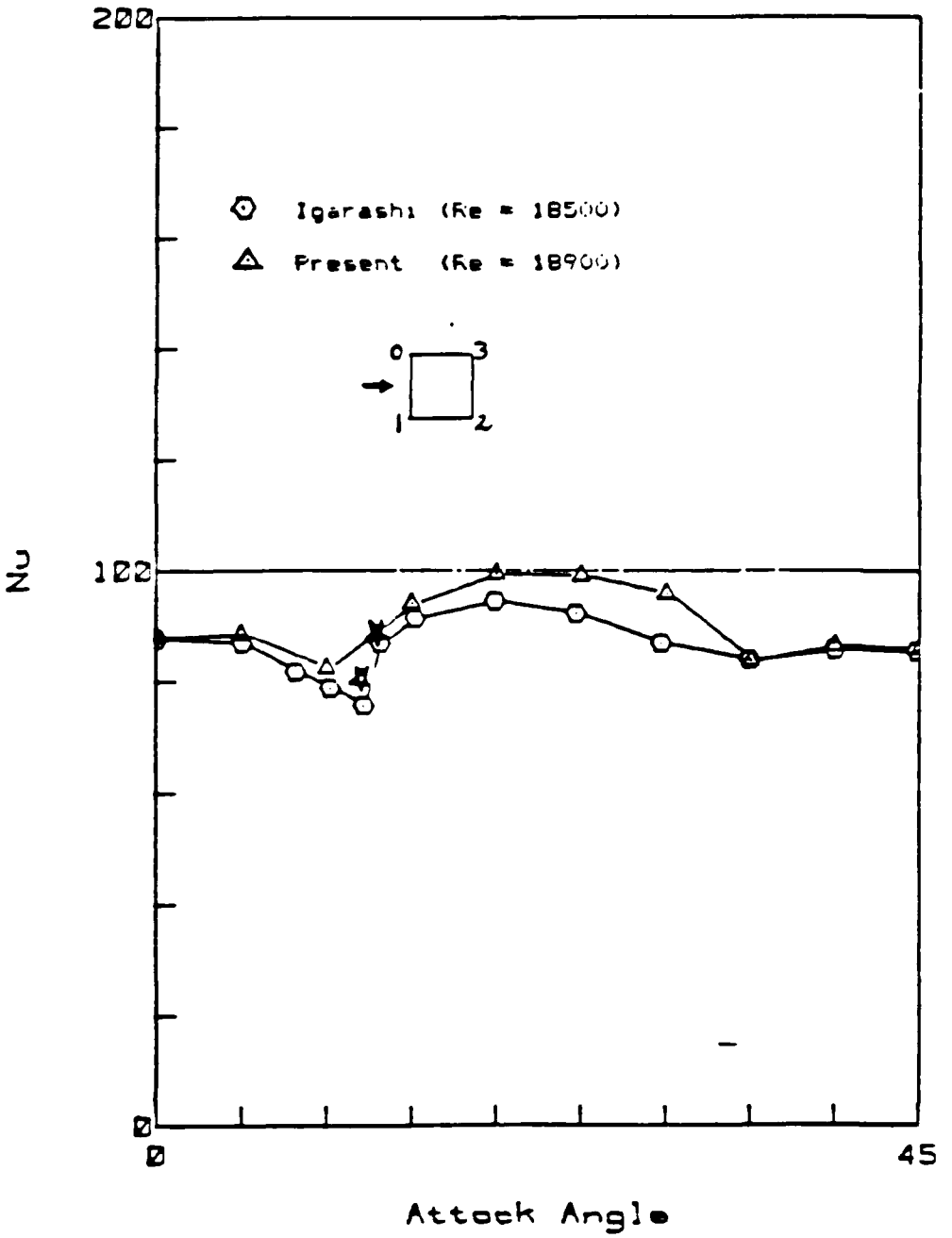

Figure E 3 - Average heat(mass) transfer rates on the square cylinder at various attack angle

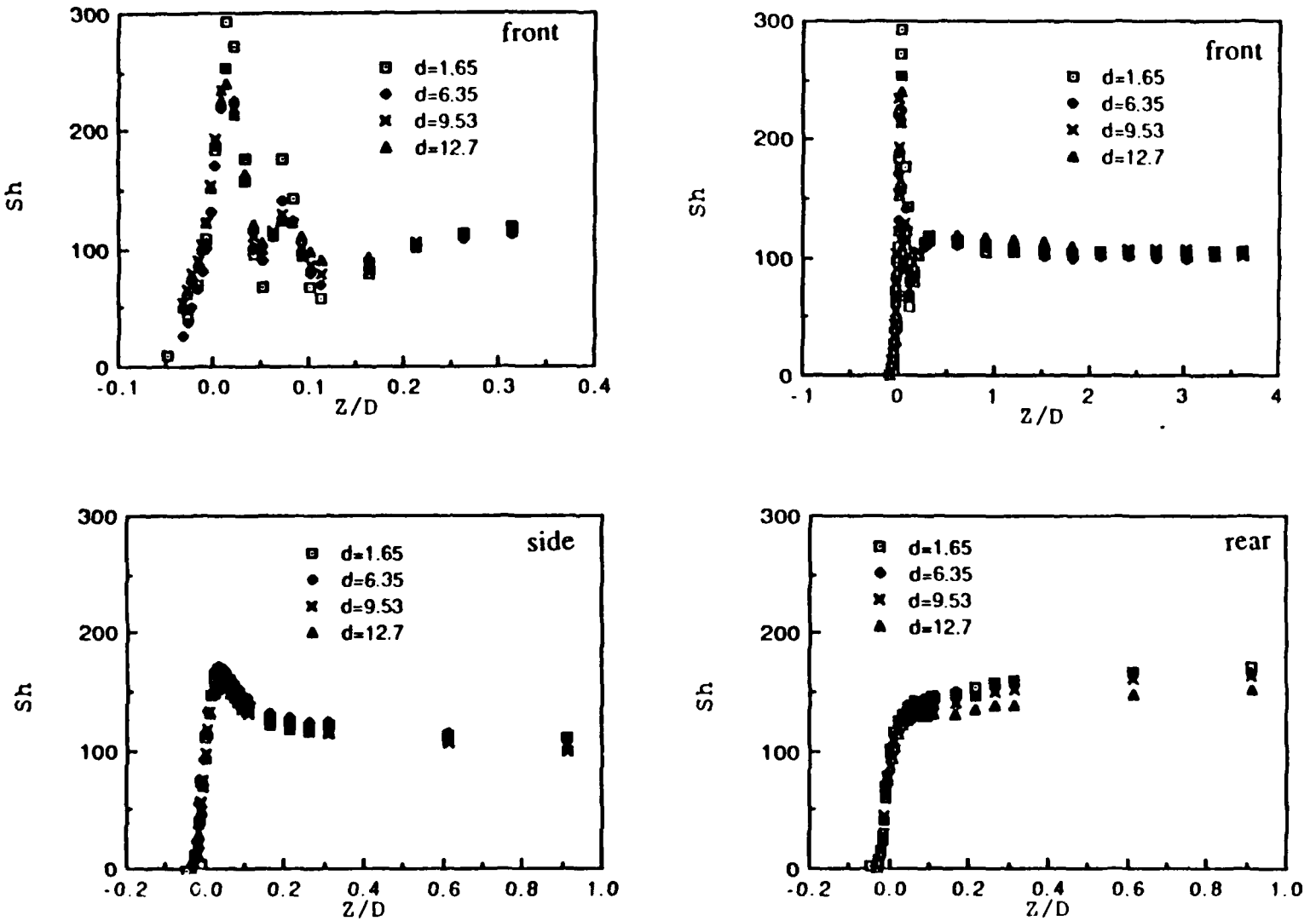

Figure E 4 - Variation of Sherwood number along the cylinder at various boundary layer thickness (U 11.7 m/sec)

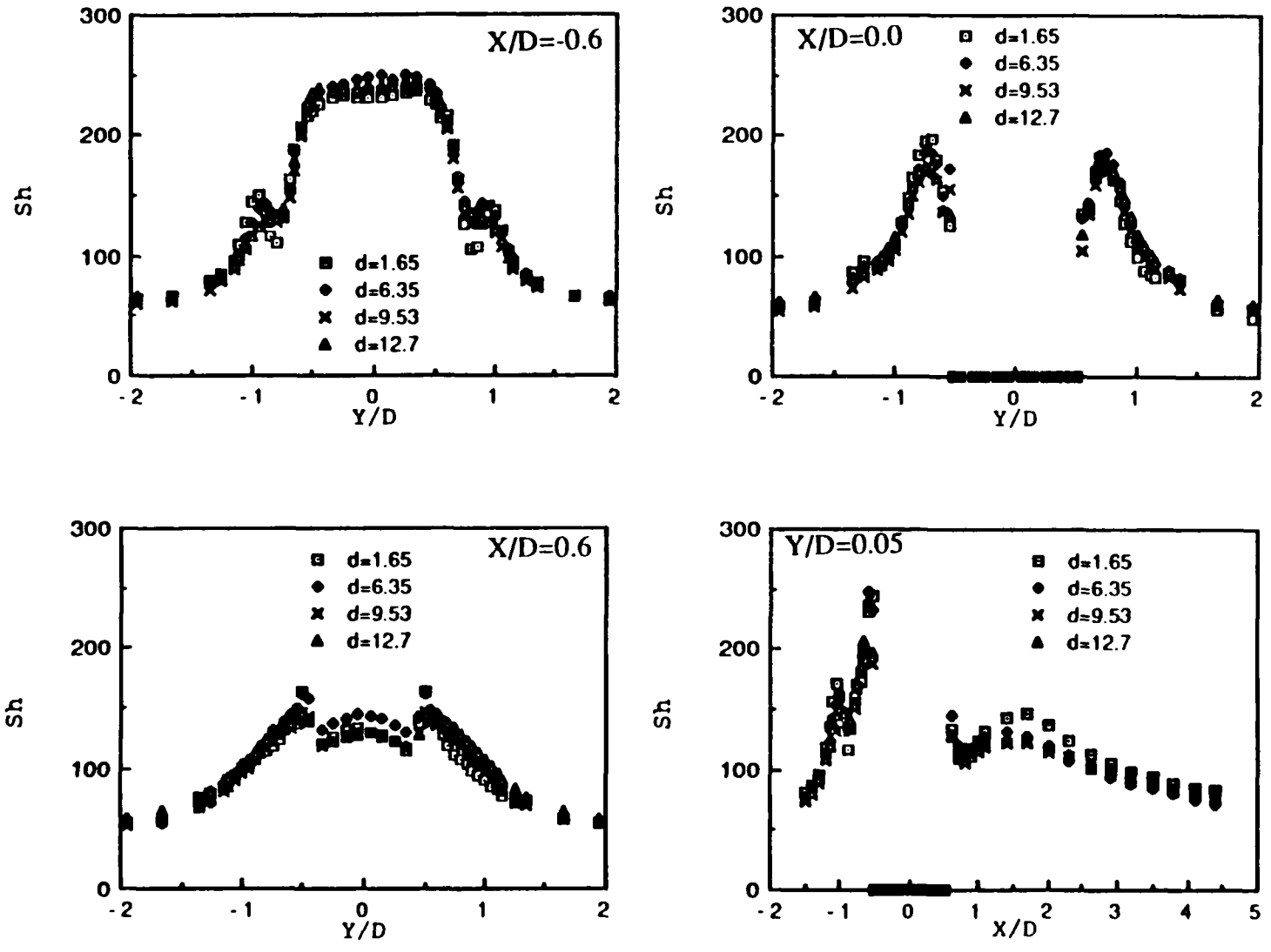

Figure E 5 - Variation of Sherwood number on the plate at various boundary layer thickness (U 11.7 m/sec)

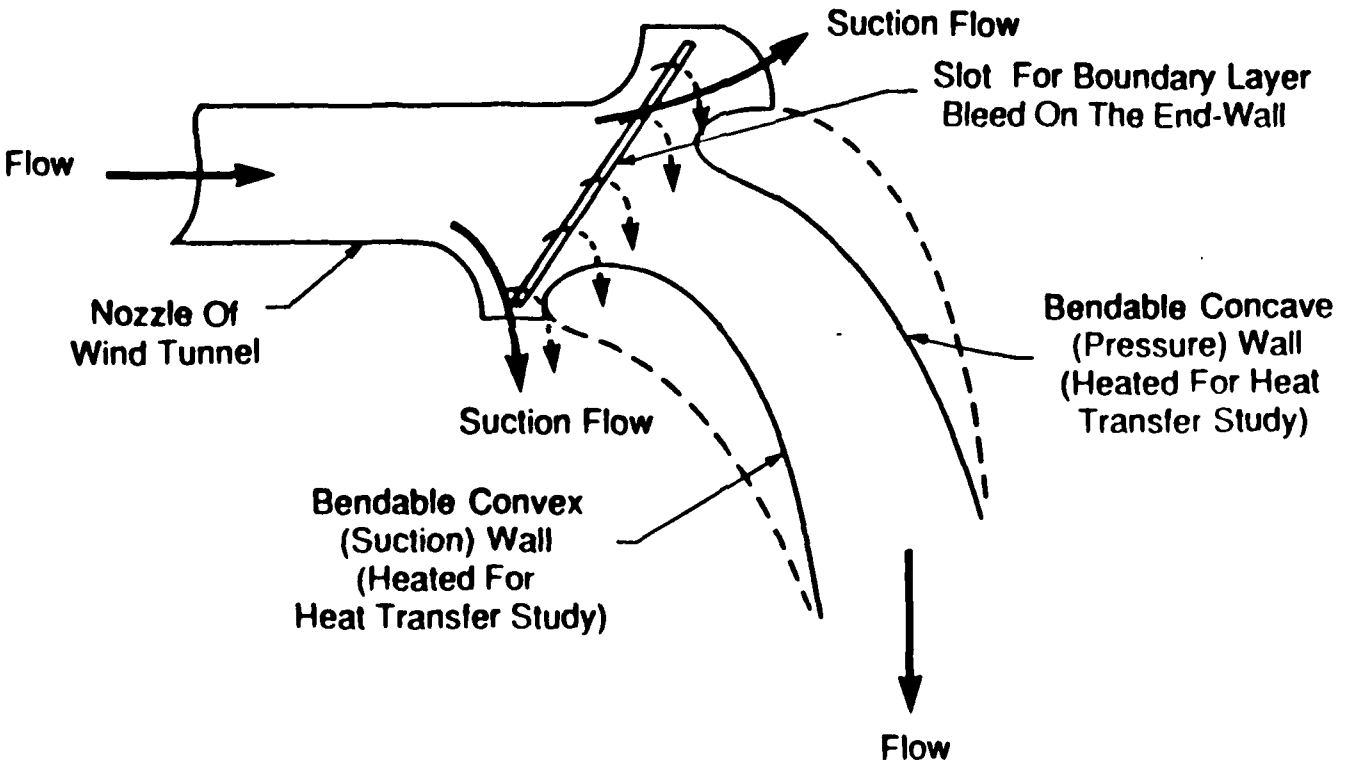

Figure F-1 Schematic of two half-blade cascade.

END

DATE

FILMED

8-88

DTIC